Structural plasticity of arrestin-G protein coupled receptor complexes as a molecular determinant of signaling

Angelo Felline [a,1], Luca Bellucci [b,1], Vanessa Vezzi [c], Caterina Ambrosio [c], Susanna Cotecchia [d], Francesca Fanelli [a,*]

[a] *Dipartimento di Scienze della Vita, Università di Modena e Reggio Emilia, via Campi 103, 41125 Modena, Italy*
[b] *NEST, Istituto Nanoscienze-CNR, Piazza San Silvestro 12, 56127 Pisa, Italy*
[c] *Istituto Superiore di Sanità, V.le Regina Elena, 299 00161 Roma, Italy*
[d] *Dipartimento di Bioscienze, Biotecnologie e Ambiente, Università di Bari, via Orabona 4, 70125 Bari, Italy*

ARTICLE INFO

ABSTRACT

G protein coupled receptors (GPCRs) are critically regulated by arrestins. In this study, high-resolution data was combined with molecular dynamics simulations to infer the determinants of β-arrestin 1 (βarr1)-GPCR coupling, using the V2 vasopressin receptor (V2R) as a model system.

The study highlighted the extremely high plasticity of βarr1-GPCR complexes, dependent on receptor type, state, and membrane environment. The multiple functions of receptor-bound βarr1 are likely determined by the interplay of intrinsic flexibility and collective motions both as a bi-domain protein and as a whole. The two major collective motions of the whole βarr1, consisting in rotation parallel to the membrane plane and inclination with respect to the receptor main axis, are distinctly linked to the two intermolecular interfaces involved in tail and core interactions.

The intermolecular dynamic coupling between βarr1 and V2R depends on the allosteric effect of the agonist arginine-vasopressin (AVP). In the absence of AVP the dynamic coupling concerns only tail interactions, while in the presence of AVP it involves both tail and core interactions. This suggests that constitutive and agonist-induced arrestin-receptor dynamic coupling is linked to distinct arrestin functions.

1. Introduction

G-protein-coupled receptors (GPCRs) control numerous cellular responses through the combined interplay of heterotrimeric G proteins, GPCR kinases (GRKs), and arrestins [1]. G proteins mediate activation of second-messenger-generating enzymes and other effectors [2], GRKs phosphorylate activated receptors [1], and arrestins subsequently bind phosphorylated receptors resulting in receptor desensitization [3]. Arrestins bound to phosphorylated receptors also serve as adaptors to link receptors to G-protein-independent signaling, i.e. activation of ERK1/2 (extracellular signal-regulated kinase), FAK (focal adhesion kinase), and Src tyrosine-kinase [3–6]. The ability of arrestins to trigger ERK signaling independently of G proteins is, however, controversial [7–10].

GPCRs are characterized by seven transmembrane (7TM) helices (H) organized in an up-down bundle architecture, with three intracellular and three extracellular loops (IL1–3 and EL1–3, respectively), as well as an extracellular N-terminus and a cytosolic C-terminus (C-tail) [11]. Most vertebrates express four arrestin subtypes: arrestin-1 (visual or rod arrestin), arrestin-2 (β-arrestin 1, βarr1), arrestin-3 (β-arrestin 2, βarr2), and arrestin-4 (cone or X-arrestin) [12].

The GPCRs vasopressin receptors (VRs) are coupled to different G proteins. The V1aR and V1bR subtypes stimulate phospholipase C by coupling to Gq/11, whereas V2R activates adenylyl cyclase by coupling to Gs [13]. In the kidneys, upon binding the agonist nonapeptide arginine-vasopressin (AVP), V2R activates the cAMP/PKA signal transduction pathway that promotes expression and trafficking of the water channel aquaporin (AQP2), thereby increasing renal water reabsorption [14]. The V2R can stimulate the ERK1/2 pathway via β-arrestins (βarrs) [9,15]. Constitutively active mutants (CAMs) of the V2R (such as R137L/C and F229V) are linked to the Nephrogenic Syndrome of Inappropriate Antidiuresis (NSIAD) [16,17], which, in contrast

---

* Corresponding author.
  E-mail address: fanelli@unimo.it (F. Fanelli).
[1] Equally contributing authors

to SIAD, is characterized by low or undetectable levels of AVP. Interestingly, these two CAMs, despite being both associated to NSIAD, display different constitutive activity towards G protein or βarr as well as different responses to ligands such as the agonist AVP and the small-molecules inverse agonists tolvaptan and satavaptan (vaptans). The R137L mutant constitutively activates Gs, is slightly constitutively coupled to βarr1, has reduced sensitivity to AVP, and does not respond to vaptan inverse agonists. In contrast, F229V is highly constitutively active towards Gs, displays higher AVP-stimulated coupling to both Gs and βarr1 compared to the wild type (WT) V2R, and responds to vaptan inverse agonists [18].

Arrestins share phosphorylation, activation, and membrane sensors, deputed to recognizing, respectively, the phosphorylated regions of the receptor, the receptor core in its active conformation, and the membrane [19]. Phosphorylation-dependent recruitment of arrestins is a common feature for GPCRs, relying on conserved phosphorylation codes [20]. The mechanism of sensing receptor phosphorylation by visual arrestin and βarr1 is very similar. Indeed, the phosphorylation codes in the C-tail of rhodopsin, PxPxxP/E/D (short code, where P is a phosphorylated serine or threonine and x is any amino acid except proline in the second xx occurrence), and of V2R (PxxPxxP/E/D (long code) are overlapping and interact with three corresponding positively charged pockets in visual arrestin and βarr1, denoted as A, B, and C [20]. The positions of such positively charged residues are highly conserved in arrestins from *C. elegans* to mammals [21]. Alanine scanning mutagenesis on rhodopsin and V2R confirmed the hypothesis that a full phosphorylation code, like those in rhodopsin and V2R, is critical for arrestin recognition [20]. Phosphorylation codes exist in all major GPCR sub-families [20]. Specifically, among 825 annotated GPCRs, 436 were found to contain full or partial codes in their C-tails. Of the 389 receptors without codes in their tails, 308 (~79 %) were found to belong to the olfactory receptor family, which recruits arrestin through phosphorylation sites within their IL3 [22]. Among the remaining 81 receptors, 48 were found to contain full or partial codes within their IL3 and comprised many members from the amine sub-family (e.g. dopamine, muscarinic, serotonin), which were shown to recruit βarrs in IL3-dependent manner [22–24]. The involvement of phosphorylated IL1 and IL2 has been documented as well [23]. Collectively, phosphorylation code analysis accounted for 96 % of the GPCR proteome [20]. Fluorescence resonance energy transfer (FRET) imaging together with focused cellular investigations showed that receptor phosphorylation patterns, in combination with receptor agonism, synergistically establish the strength and specificity with which diverse downstream βarr-mediated events are directed [25].

For those receptors like V2R, which hold phosphorylation codes in their C-tail, it has been hypothesized a stepwise process of arrestin-receptor recognition, in which arrestin would first bind to the phosphorylated receptor C-tail appearing to hang from the receptor (tail/hanging conformation) and successively bind concurrently to the receptor intracellular core (core conformation) [26,27]. In the tail conformation, the receptor intracellular core is potentially available for interaction with G protein to form a receptor-G protein-βarr 'megacomplex' able to stimulate G protein signaling while being internalized by βarr [26,28].

The interactions of arrestin with the phosphorylated GPCR C-tail to form the interface-1, with the GPCR core regions to form the interface-2, and with the membrane, all help determining the conformational ensemble, which underlies the multiple arrestin functions [15]. For those receptors with phosphorylation codes in the intracellular loops and not the C-tail, arrestin recruitment likely relies on core interactions. While the engagement of only the phosphorylated tail preserves the ability to mediate receptor internalization and βarr signaling, desensitization of G protein signaling requires the additional engagement of the receptor core [29]. The cryo-electron microscopy (cryoEM) complex between βarr1 and glucagon-bound glucagon receptor (GCGR)/V2R C-tail (V2RCt) shows a high-resolution view of a tail conformation, characterized by the interface-1 and additional interactions between the

central-crest of βarr1 and H8 of the receptor but not the receptor core [30]. Data strongly implied that the tail conformation of βarr1 is largely involved in the cellular trafficking of GCGR [30]. Differently from the tail conformation emerged by the single-particle EM analysis of the βarr1-β2 adrenergic receptor (AR)/V2RCt complex, in which βarr1 is perpendicular to the membrane [27], in the complex with GCGR, βarr1 forms a 45° angle with the membrane plane [30]. A combination of in vitro and computational experiments on visual arrestin-rhodopsin interaction showed that binding to the receptor tail and the receptor core can each independently cause the global conformational changes in arrestin required for activation [31]. A distinct and additional mechanism of βarr activation that does not require stable βarr scaffolding or the GPCR tail has been demonstrated as well [32]. It occurs through transient engagement of the GPCR core, which promotes capture of βarr at the plasma membrane and its accumulation in clathrin-coated endocytic structures [32]. Single-molecule experiments showed that βarr spontaneously pre-associates with the plasma membrane, allowing it to explore space via lateral diffusion and to undergo highly transient interactions with receptors that lead to βarr activation [33].

To gain insight into the molecular determinants of receptor-arrestin coupling, in the present study, all information from structure determination available so far on βarr1 in its isolated inactive state or in complex with phosphorylated GPCRs [26,34–42] was integrated with atomistic microsecond molecular dynamics (MD) simulations of hexaphosphorylated V2R in ternary complex with AVP and βarr1. V2R was modeled in its WT form and in the two NSIAD-linked R137L and F229V mutant forms. The two mutants were also simulated in their apo states. The choice of the βarr1-V2R complex as a model system was because of the huge availability of valuable information on the recognition between the two proteins, considering also the fact that the V2R V2RCt provides the GPCR with high-affinity binding to βarrs [43]. The effects of phosphorylation extent and membrane shape on the architecture and dynamics of βarr1-V2R complex were also inferred by comparing the results of present simulations with previous simulations on an octaphosphorylated version of V2R [44] and with the cryoEM complex of βarr1-V2R in lipid micelles [40] released when simulations were completed.

Collectively, the results of the present integrative molecular modeling study provide significant insights into the dynamic coupling of βarr1 and V2R under the allosteric effect of the AVP agonist and the interactions with the membrane.

2. Material and methods

2.1. MD simulations

2.1.1. Model building of the ternary complex

The input structural complex between V2R and βarr1 was achieved by integrative molecular modeling. The CryoEM structure of the V2R in complex with heterotrimeric Gs (Protein Data Bank (PDB): 7DW9) [45] was fitted onto the CryoEM structure of the β1AR/phosphorylated V2RCt chimera (β1AR) in complex with βarr1 (PDB: 6TKO) [38]. When we started modeling and simulations, the available cryoEM complexes between βarr1 and a GPCR holding the V2RCt were the 6TKO and 6UON structures, both solved in nanodiscs. We selected 6TKO because it had a significantly higher resolution than 6U1N. Today, despite the availability of more cryoEM complexes, all solved into micelles, we would confirm our original choice because nanodisks are more similar in shape than micelles to the membrane model employed in our simulations. The V2R structure hence added of the phosphorylated V2RCt from the 6TKO complex was subjected to completion of EL2, IL2, IL3, and the C-tail (by the loop_model routine of Modeller [46]). As already stated in a previous report, IL3 was in great part modeled as a cytosolic protrusion of H5 and H6 [44]. During comparative modeling, α-helical restraints were applied to the following amino acid stretches: 143–151 (in IL2), 231–246 (cytosolic extension of H5), 253–267 (cytosolic extension of H6), and

334–341 (H8).

Upon addition of the missing residues 332–340 (by Modeller), βarr1 from the β1AR-βarr1 (6TKO) complex was added to the completed model of V2R.

A final structural model of V2R phosphorylated at pS357 (phosphorylation site 3 (p3), Supplementary Table 1 (Table S1)), pT359 (p4), pT360 (p5), pS362 (p6), pS363 (p7), and pS364 (p8) and palmitoylated at C341 and C342 (at the C-terminus of H8) in complex with βarr1 was achieved. MD simulations concerned such complex in the WT form or carrying the R137L or F229V NSIAD-linked mutations in complex with the peptide agonist AVP (from the original CryoEM 7DW9 complex [45]). The apo forms of the two V2R NSIAD mutants in complex with βarr1 were simulated as well.

The agonist AVP is a cyclic peptide due to a disulphide bridge between C1 and C6. In the structure used as an input of MD simulations, it docks on the EL2 β-hairpin and makes a number of inter-molecular interactions with V2R amino acid residues, e.g. those in: N-term (R8$_{AVP}$-D33$_{V2R}$), H1 (R8$_{AVP}$-E40$_{V2R}$), H2 (Q92$_{V2R}$-Y2$_{AVP}$-Q96$_{V2R}$), EL1 (G9$_{AVP}$-R104$_{V2R}$), H3 (F3$_{AVP}$-M129$_{V2R}$), EL2 (N5$_{AVP}$-W193$_{V2R}$), H5 (V206$_{V2R}$-F3$_{AVP}$-I209$_{V2R}$ and Q4$_{AVP}$-R202$_{V2R}$), H6 (Q4$_{AVP}$-Q291$_{V2R}$-F3$_{AVP}$-F287$_{V2R}$, F3$_{AVP}$-F288$_{V2R}$, and Y2$_{V2R}$-F287), and H7 (C1$_{AVP}$-M311$_{V2R}$). Those interactions are slightly different in the cryoEM complex between V2R and βarr1 (PDB: 7R0C), essentially due to the different conformation of the peptide C-tail. The flexibility of the AVP C-tail emerges also from structure comparisons of the peptide from other cryoEM complexes between V2R and Heterotrimeric Gs (PDBs: 7BB6 and 7BB7 [47]).

2.1.2. MD simulation setup

The structural models of WT and mutated V2R in ternary complex with AVP and βarr1 were used as inputs of MD simulations. The apo mutants R137L and F229V were also simulated in binary complex with βarr1.

The N-termini of both βarr1 and V2R were acetylated, whereas the C-termini of βarr1, V2R, and AVP were amidated. Two disulphide bridges were allowed to form between C112(3 × 25) (the labeling in parenthesis refers to a positional numbering widely used for GPCRs [48,49]) and C192 in V2R EL2 and between C1 and C6 both in AVP. Furthermore, the highly conserved D85(2 × 50) and D136(3 × 49) from V2R were kept in their protonated (neutral) states, consistent with evidences on the corresponding amino acid residues in rhodopsin [50,51].

Simulations were performed by NAMD2.11 [52] and were conducted in the NPT (constant particle Number, Pressure, and Temperature) ensemble. Periodic boundary conditions (PBC) were used and the long-range electrostatic interactions were treated with the particle-mesh-Ewald (PME) method [53]. The cutoff for non-bonded interactions was set to 10 Å and the switching function was applied to smooth interactions between 9 and 10 Å. The bonds between hydrogens and heavy atoms were constrained using the SHAKE algorithm [54], allowing for an integration step of 2 fs. The r-RESPA multiple time step method [55] was employed, allowing to update long-range electrostatic interactions every 4 fs and all the other interactions every 2 fs. The temperature was set to 310 K and regulated via a Langevin thermostat, while pressure was set to 1 atm and regulated via an isotropic Langevin piston manostat (as implemented in NAMD). The CHARMM36 force field was used for protein, membrane, phosphoryl, and palmitoyl groups, and counterions, and the TIP3P model [56] was used for the water solvent.

Phosphorylated and palmitoylated V2R in complex with both AVP and βarr1 was placed in the center of a phosphatidylcholine (1-palmitoyl-2-oleoyl-sn-glycero-3-phosphocholine, POPC) membrane generated exploiting the VMD Membrane Builder plugin [57] (Supplementary Fig. 1 (Fig. S1)). Lipids within 1 Å from the protein complex were removed and the complex was placed along the z-axis so that the center of mass of the receptor coincided with the center of the membrane. The POPC-embedded protein complex was then solvated and neutralized with 59 Na$^+$ and 64 Cl$^-$, reaching a salt concentration of about 0.05 mol/L. The final system was simulated in a cubic box of 150x150x150

Å^3, which ensures correct decoupling between the periodic replica; the maximum extension of the whole protein complex was not greater than 110x110x110 Å^3.

Energy minimization was carried out, followed by 4-ns equilibration of the membrane around the protein, while keeping the protein heavy atoms harmonically constrained to their initial positions. The constraints over the protein were then removed and the system was further minimized. After minimization, the system was equilibrated for 100 ns. Box dimensions in the equilibrated system were about 138x138x137 Å^3. Such equilibration was followed by 1.0 μs production, by keeping the dimensions of the unit cell constant in the xy-plane, while allowing fluctuations along the z-axis.

During the production stage, distance restraints were applied to maintain selected inter-molecular contacts or secondary structures in V2R, according to experimental evidence [58–60]. In detail, α-helical restraints between the backbone oxygen atom at position i and the backbone nitrogen atom at position i + 4, excluding proline residues, were applied to a) the segment 144–150 in IL2; and b) the segments 230–242 and 254–267 in cytosolic ends of H5 and H6. Furthermore, antiparallel β-sheet restraints were applied to the H-bond-forming sites of the EL2 β-hairpin (i.e. positions 179 and 181 in the N-terminal strand paired, respectively, with positions 191, and 193 in the C-terminal strand). Finally, distance restraints were also applied between selected atoms of V2R and AVP such as: a) respectively D33 (OD1) and R8 (NH1), A194 (N) and N5 (OD1), R202 (NH2) and Q4 (OE1), as well as Q291 (OE1) and Q4 (NE2).

2.2. MD analyses

All structural analyses were carried out by the in-house software Wordom [61,62] and PSNtools [63].

For each simulated V2R form, comparative structural analysis concerned either the whole conformational ensemble from MD simulations or the trajectory frame closest in Cα-atom root mean square deviation (Cα-RMSD) to the average structure (i.e. representative of the conformational ensemble, hereafter named Rframe).

2.2.1. Analysis of structural deformations and collective motions

MD trajectories were subjected to a variety of analyses by the Wordom software [61,62] aimed at computing: a) geometrical and size/shape descriptors, e.g. inter-atomic distances, intra- and inter-molecular angles, and solvent accessible surface area (SASA); b) intrinsic flexibility, e.g. Cα-RMSD, Cα-atom root mean square fluctuations (Cα-RMSFs), force constants [64–66], overall fluctuations [67], invariant core [68], and geometrically stable domains, by GeoStaS [69]; and c) collective motions by the principal component analysis (PCA) of the atomic fluctuations [70]. Only the most meaningful results are shown.

For estimating the strength and extension of the interfaces-1 and 2, the missing side chains and all hydrogens were added to the cryoEM structures by means of the Chimera molecular visualization software [71]. Side-chain conformations were assigned by a mixture of rotamer libraries, i.e. the Dunbrack and Karplus (D&K) [72] and Ponder and Richards (P&R) [73]. The C-tail of the neurotensin receptor 1 (NTSR1) was phosphorylated at S409, S410, T413, and T416, according to experimental evidence [37].

2.2.2. Structural communication by the protein structure network analysis

The structural communication was investigated by the protein structure network (PSN) analysis implemented in the PSNtools [63]. PSN analysis is a product of graph theory applied to protein structures [74]. The methodological approach for computing the structure graph and the shortest communication pathways has been described in a number of research articles [63,75,76].

Shortly, in a PSN, each linked residue (e.g. amino acid, nucleotide, small molecules, ion, etc) is a node [77]. Links form if the non-covalent interaction strength between pairs of nodes equals or overcomes a cutoff

(I_min). Such interaction strength, expressed as a percentage, is computed by the Eq. (1) below:

$$I_U = \frac{n_{ij}}{\sqrt{N_i N_j}} \times 100 \qquad (1)$$

where I_{ij} is the percentage interaction between residues i and j; n_{ij} is the number of heavy atom-atom pairs between the side chains of residues i and j within a distance cutoff (4.5 Å); N_i and N_j are normalization factors for residue types i and j, which account for their propensities to make contacts with surrounding residues [74,78]. As for the normalization factors, the PSNtools software employs an internal database holding the normalization factors for the 20 standard amino acids and the 8 standard nucleotides (i.e. dA, dG, dC, dT, A, G, C, and U), as well almost 40,900 molecules (e.g. small molecules, lipids, sugars, etc) and ions extracted from all the structures deposited to date in the PDB.

Thus, the interaction strengths (I_{ij}) are computed for all node pairs. At a given interaction strength cutoff, I_{min}, any residue pair ij for which $I_{ij} \geq I_{min}$ (see eq. 1) is considered interacting and hence is connected. The I_{min} cutoff is automatically computed as described in a recent paper [63]. In more detail, the I_{min} employed for the PSN analysis on MD simulations is the average over all the I_{min} computed on each trajectory frame.

Only those links and hubs present in at least 50 % of the trajectory frames were defined as stable and considered for further analysis.

To avoid excessive network fragmentation, which would impair the search for the shortest communication pathways, all node clusters (i.e. ensembles of nodes connected by at least one link) were iteratively connected by the link with the highest sub-cutoff interaction strength.

Allosteric communication was studied by searching for the shortest communication pathways. A pathway describes how signals are
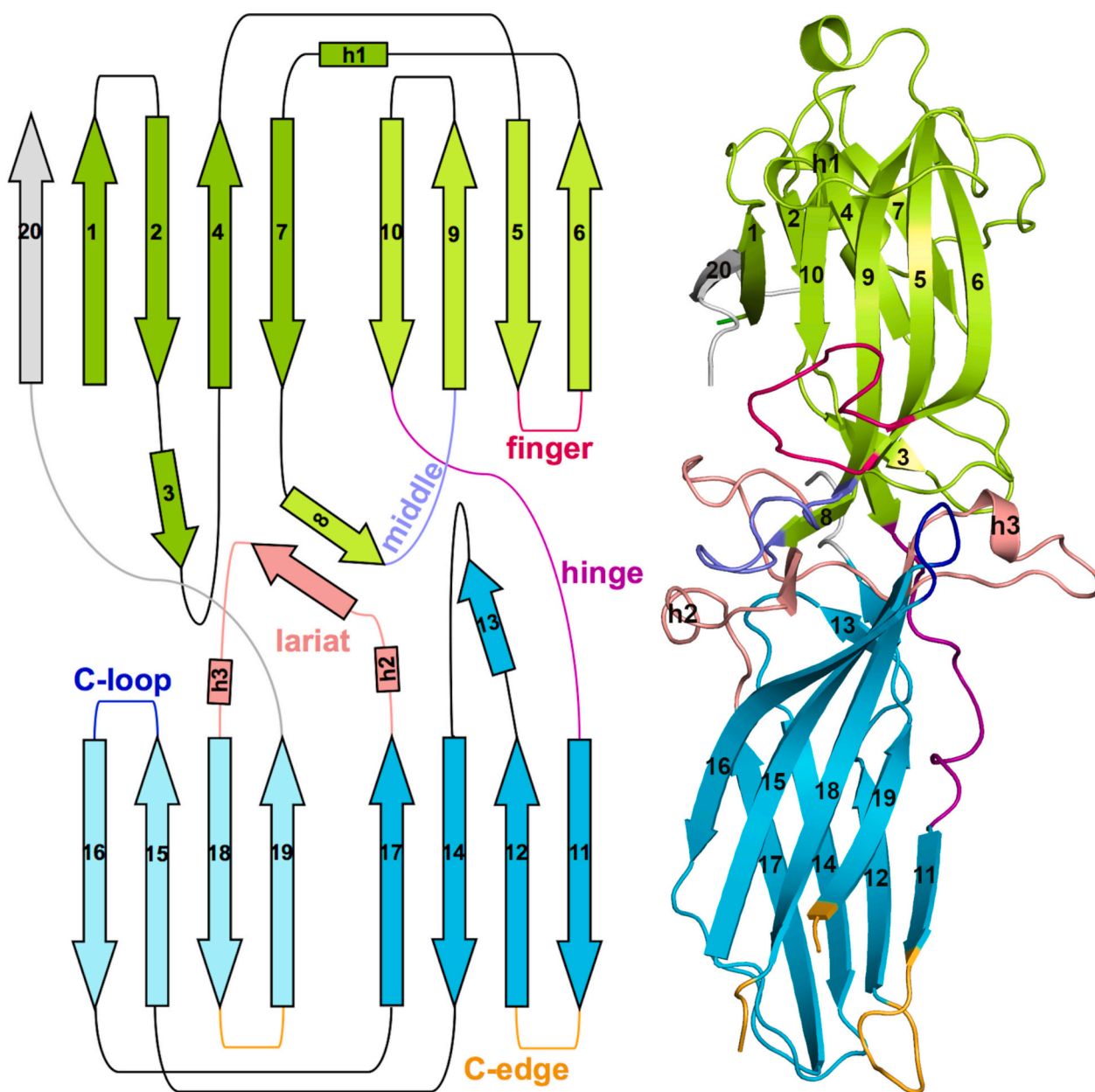
Fig. 1. Topology diagram of inactive βarr1. The topology diagram of inactive βarr1 is shown on the left while cartoons of the 3D structure 1G4M are shown on the right colored according to the topology diagram. As for coloring, ND and CD are lemon-green and cyan, respectively, whereas the last strand (β20) is gray; finger, middle, C-, lariat, and C-edge loops and the hinge inter-domain linker are, respectively, hotpink, slate-gray, salmon-pink, blue, bright-orange, and purple. (For interpretation of the references to colour in this figure legend, the reader is referred to the web version of this article.)

transferred between sites and consists of a set of residues in dynamic contact [79,80]. The procedure for computing the shortest communication pathways, which has been previously described and validated [63,76], is based on Dijkstra's algorithm [81]. The motion correlation cutoff of 0.8 was used for path filtering [63,76].

A coarse/global picture of the whole structural communication in the considered system is provided by consensus paths or metapaths made of the most recurrent links in the path pool (i.e. with a recurrence ≥20 % in this study) [63].

In this study, the PSN analysis was used to compute the global strength of the links at the two βarr1-receptor interface and the metapaths from the shortest communication pathways that involve at least one node in AVP and its binding site.

3. Results

3.1. Analysis of MD simulations in the framework of high-resolution data on βarr1-GPCR complexes

3.1.1. Structural features of βarr1 and βarr1-V2RCt interface

βarr1 holds a β-sandwich architecture and an immunoglobulin-like topology made of one N-terminal (residues 6–172) and one C-terminal (residues 185–359) domains (ND and CD, respectively) (Fig. 1). Each domain consists of two sheets made of four antiparallel β-strands packed against each other (i.e. 1,2,4,7 and 6,5,9,10 for the ND and 11,12,14,17 and 16,15,18,19 for the CD). The two domains are connected by a 12-residue hinge (residues 173–184), which is involved in the inter-domain twist linked to arrestin activation [82]. In the inactive state, the last strand in the C-terminal tail makes a parallel sheet with the β1-strand in the ND (Fig. 1). Three extra-sheet strands, β3, β8, and β13 form anti-parallel sheets with β10, the lariat loop (residues 275–318 in the CD), and the C-tail (Fig. 1).

Three short helices, which do not contribute to the class and architecture of the domains, are present: one in the β6/β7 loop (h1) and two in the lariat loop (h2 and h3) (Fig. 1).

Two intra-sheet loops, finger loop (residues 63–75 in the ND) and C-loop (residues 242–246 in the CD), and two inter-sheet loops, middle loop (residues 130–140 in the ND) and lariat loop, participate in the central crest involved in receptor recognition (Fig. 1). The lariat loop comprises the gate (residues 289–298) and back loops (residues 311–318). The CD holds two edge loops (β11/β12 loop, residues 189–196, and β18/β19 loop, residues 330–342; Fig. 1), deputed, with emphasis on the β18/β19 loop, to interactions with the membrane (Fig. 1 and S1).

A number of βarr1 structures in different functional states are currently available. The solved states include the inactive state and the active states bound to the phosphopeptide from the C-tail or to both the C-tail and the core of a number of GPCRs (Tables S1 and S2). Herein, the 1G4M structure (Fig. 1 [34]) was used as a representative of the inactive state in comparison with a number of active-state structures. As for the βarr1 state bound to the receptor C-tail phosphopeptide, the following complexes with a variedly phosphorylated V2RCt (i.e. with only interface-1 formed) were considered: a) fully-phosphorylated (octa-phosphorylated) structure (4JQI_pp8 (i.e. a phosphopeptide with eight phosphoryl groups), Fig. S2A) [35]; b) hepta-phosphorylated (7DF9_pp-1, i.e. with un-phosphorylated site 1, 7DFC_pp-3 and 7DFA_pp-5, Fig. S2B-D and Table S1 [36]); and c) hexaphosphorylated (7DFB_pp-7,8 [36] and 6NI2_pp-1,2 [26], Fig. S2E, F, and Table S1).

In all βarr1-GPCR/V2RCt complexes holding both interfaces-1 and 2, the phosphoryl groups solved at the atomic detail are six (i.e. in 6TKO, 6U1N, and 7R0C Fig. S3A—C)) or five (i.e., in 8WRZ, Fig. S3D). Liquid chromatography-tandem mass spectrometry (LC–MS/MS) on the β2AR-V2RCt chimera revealed that while the N-terminal T347 and S350 are always phosphorylated independent of receptor stimulation and are not essential to βarr1 recruitment, S357, T359, T360, and S362 are instead phosphorylated by GRK upon agonist stimulation and are essential to

βarr1 recruitment [26].

Comparative analysis of the interface-1 involving variedly phosphorylated V2RCt shows high structural similarity among all compared complexes, independently of the degree of V2RCt phosphorylation (Figs. S2 and S3). Indeed, the last six phospho-serine/threonine residues of V2RCt recognize three cationic sites on βarr1, i.e. sites A (K11 and R165), B (K11, R25, and K294), and C (R7, K10, and K107) (Figs. S2 and S3). Incidentally, the only residue in the cationic sites that belongs to CD is K294 in the lariat loop (specifically in the gate loop). In detail, pS357 interacts with site A, pT359 and pT360 interact with site B, and pS362, pS363, and pS364 interact with site C. The first two phosphorylated amino acid residues, pT347 and pS350 (p1 and p2 sites), where present, recognize, respectively, an additional cationic site D involving both finger loop (R65 and K77) and site A (Fig. S2A,C-E). Thus, in all βarr1-V2RCt complexes, in which the p1 and/or p2 sites are phosphorylated and only the interface-1 can form, the V2RCt makes tight interactions with the finger loop (Fig. S2A-E). In contrast, in all βarr1-receptor complexes holding both interfaces-1 and 2, the p1 and p2 sites are not solved. In those complexes, the orientation of the finger loop, which effectively participates in the interface-2, is such that even if phosphorylated, the p1 and p2 sites would likely not contribute to the interface-1 (Fig. S3). Remarkably, the intermolecular interactions characterizing the phosphorylated residues at the interface-1 are conserved also in the complex between βarr1 and the Class-B GCGR in tail conformation [30].

In summary, upon binding to βarr1, the V2RCt extends the first sheet of the β-sandwich by making an anti-parallel β-sheet with the β1, thus displacing the C-terminal β20-strand. This binding mode is the result of a general mechanism, by which arrestins recognize the C-terminal tails of receptors, leading to formation of the interface-1, which triggers βarr1 activation [35]. Indeed, displacement of the βarr1 C-tail by the receptor V2RCt, which is used as a marker of arrestin activation [25], triggers conformational changes of the central loops and a 20°-twisting of the ND and CD around the βarr1 main axis [27], thus disrupting two sets of intra-molecular constraints: a) the interactions among β1, α1, and the C-tail of arrestin (three-element interaction [83]); and b) the polar core consisting of five interacting charged residues: D26, R169, D290, D297, and R393 [84,85]. Notably, the side chain of K294, a residue within the gate loop, flips towards the ND upon activation and engages pT360 of V2RCt as a consequence of a conformational change in the loop. Comparisons of inactive (1G4M) and V2RCt-bound active (4JQI) βarr1 led to the hypothesis that the interaction of K294 with the C-tail phosphates provides an additional driving force for the lariat-loop rearrangement associated with βarr1 activation [35]. More recent site-directed mutagenesis of the conserved lysine in arrestin-1, -2, and -3 suggests that it participates in receptor binding, but does not play a critical role in phosphate-induced arrestin activation [86].

3.1.2. Structure comparisons of cryoEM and simulated βarr1-GPCR complexes made of both C-tail and core interactions

The first atomistic view of receptor-arrestin core interactions was provided by X-ray laser-crystallographic structure determinations of the complex between pre-activated visual arrestin and constitutively active opsin [87]. The structure revealed that the ~20° interdomain twisting opens a cleft in arrestin to accommodate a two-turn helix formed in IL2 of the receptor, thus allowing core interactions [87], which were later confirmed by the cryoEM complexes between βarr1 and several GPCRs [12].

The structural analysis of the existing βarr1-receptor complexes was exploited herein to drive the analysis of the conformational ensembles from microsecond MD simulations of βarr1 in complex with AVP-bound WT and mutated V2R. The two NSIAD-linked mutants R137L and F229V concern, respectively, the arginine of the conserved E/DRY motif at position 3 × 50 and a phenylalanine at position 5 × 62. In the WT Rframe, R137 is folded, being involved in interactions with both E66 and D69 in the finger loop of βarr1, whereas F229 is involved in inter-

helical van der Waals interactions with V240 (at position 6×34). The two mutants were also simulated in their apo states (R137L$_{APO}$ and F229V$_{APO}$).

The rather high homogeneity of the interface-1 contrasts with the high structural variability of the interface-2 (Figs. S2-S4). The latter is contributed by the central-crest loops and the C- and N-terms, respectively, of β15 and β16 of βarr1 and the cytosolic ends of H3, H5, and H6, the N-term of H8, and the three intracellular loops (IL1–3) of the receptor (Fig. S4).

All existing cryoEM complexes holding the interface-2 were considered in the comparative structural analysis, being listed according to the release-date: βarr1-NTSR1 (or NTS1, PDB: 6PWC [37]), βarr1-β1AR (PDB: 6TKO) [38], βarr1-M2 muscarinic receptor (M2R or M2, PDB: 6U1N [39]), βarr1-V2R (or V2, PDB: 7R0C [40]), βarr1-5HT2B serotonin receptor (5HT2BR or 5HT2B; PDB: 7SRS [41]), and βarr1-CB1-cannabinoid receptor (CB1R or CB1, PDB: 8WRZ [42]) (Tables S1 and S2). It is worth recalling that, although the cryoEM structures listed above contain stabilizing mutations on βarr1 and/or the GPCR, and are receptor/V2RCt chimeras in three cases, all constructs proved to be functional in G protein coupling and/or in arrestin-mediated receptor internalization under the effect of the specific agonist (see the relative articles). A greater artifact could have been M2R_6U1N that, being an M2R/V2RCt chimera, is phosphorylated at the C-tail, whereas in nature M2R is phosphorylated at the IL3 [24]. That was not the case. In fact, βarr1 was found to enhance the affinity of agonists for M2R/V2RCt to the same extent as for natively phosphorylated M2R [39]. Moreover, the possibility that phosphorylated IL3 residues influence the relative orientation of βarr1 seems unlikely given the length of this loop (152 residues) and its lack of order in the cryoEM structure [39].

Collectively, all observations above give value to the cryoEM data exploited in the present analysis.

As already stated in the Introduction, the 7R0C structure of the βarr1-V2R complex was released when the current MD simulations were completed. Remarkably, the resolution of 7R0C is such that several relevant regions are missing, i.e. portions of EL2, IL2/H4 N-term, IL3, and the whole N-terminus, and the whole C-tail but the 356–368 terminal stretch of V2R and part of the β18/β19 loop of βarr1. Moreover, the high inclination of βarr1, due to its interaction with a curved lipid micelle, is not compatible with a realistic interaction with a rather planar cell membrane, like the one employed in present simulations.

The high divergences in the architectures exhibited by the interface-2 are due, in part, to the structural variability of the central-crest loops of βarr1, the cytosolic regions of GPCRs (in particular, IL2, the cytosolic extensions of H3, H5 and H6, and the N-term of H8), and βarr1 interaction with membranes (Fig. S4). Remarkably, the finger loop assumes different conformations in all cryoEM complexes, holding differently-oriented one-turn α-helix in NTSR1_6PWC, 5HT2BR_7SRS, and CB1R_8WRZ and random conformations in the others (Fig. S4). Major structural differences in the interface-2, however, reside in the orientation of βarr1 with respect to the receptor. This clearly emerges from the Cα-RMSD matrices shown in Figs. 2 and S5. Indeed, the Cα-RMSDs computed either on the receptor or βarr1 (Fig. S5) are significantly lower (i.e. up to 4.24 Å) than those computed on the whole complex (up to 39.89 Å, Fig. 2). The highest values concern NTSR1_6PWC, the Cα-RMSDs ranging from 25.42 Å to 39.89 Å (Fig. 2).

As for the structural comparisons of the V2R WT Rframe from MD simulations and the cryoEM complexes, fitting and computing the Cα-RMSD on either the receptor or βarr1 (Fig. S5 lower and upper triangular matrix, respectively) shows, respectively, the highest similarities with βarr1 from β1AR_6TKO (Cα-RMSD: 2.12 Å) and the V2R from V2R_7R0C (Cα-RMSD: 2.27 Å), which is consistent with the fact that in the input complex of MD simulations βarr1 derives from β1AR_6TKO, whereas V2R comes from the cryoEM complex with heterotrimeric Gs (PDB: 7DW9) (Fig. 2). As for the Cα-RMSDs computed on the whole complexes, the highest similarity is always reached with the β1AR_6TKO employed as a template to build the input complex (Cα-RMSDs: 3.87 Å and 6.82 Å
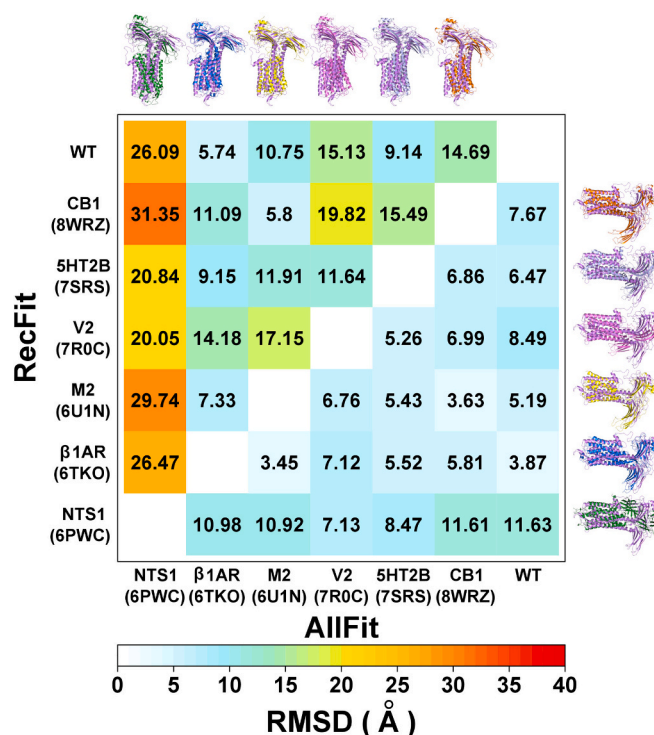

Fig. 2. Structural comparisons of the cryoEM βarr1-receptor complexes. The pairwise Cα-RMSD matrix concerning six cryoEM complexes (indicated by the PDB code) and the most representative frame (Rframe) from MD simulations of WT V2R (WT) is shown. Values below the diagonal were obtained by fitting and calculating the RMSD on all Cα atoms. In contrast, those above the diagonal were obtained by fitting the Cα-atoms of the receptor and calculating the RMSD on the Cα-atoms of βarr1. Above and on the right side of the matrix, the cartoon representations of WT superimposed on each cryoEM complex are shown. As for coloring, WT, 6PWC, 6TKO, 6U1N, 7R0C, 7SRS, and 8WRZ are lithium-violet, forest-green, marine-blue, yellow, violet, light-blue, and orange, respectively. (For interpretation of the references to colour in this figure legend, the reader is referred to the web version of this article.)

in the lower and upper triangular matrices, respectively, Fig. 2). For each trajectory, the Cα-RMSDs with respect to the first frame show median values up to 2.54 Å, the highest flexibility concerning F229V$_{APO}$ (Fig. S6). Comparisons of the mutant trajectories with the WT Rframe show Cα-RMSD median values around 4 Å for R137L$_{APO}$, R137L, and F229V$_{APO}$, which increase for the AVP-bound F229V (i.e. 6.07 Å median value, Fig. S6).

Collectively, structure comparisons of all cryoEM complexes and the V2R Rframes from MD simulations indicate that the structural divergences essentially reside in the orientation of βarr1 with respect to the GPCR and the membrane plane.

3.1.3. Structural plasticity of βarr1-GPCR complexes

A combination of structural indices proved able to comprehensively account for the variability in βarr1-receptor complexes (Figs. 3–5 and S7, Table S2). These indices include: a) Dist, the minimal distance between the geometrical center of the βarr1 C-loop and any Cα-atom in receptor H5; b) Tilt, the angle between the major axes of the receptor and βarr1, representing the inclination of βarr1 with respect to the receptor-main axis; c) Twist, βarr1 inter-domain twist angle; d) Rot, the angle between the major axes of receptor H8 and βarr1, representing the rotation of βarr1 parallel to the membrane plane; e) Int1 and Int2, the summations of the interaction strengths of all links at the interface-1 and the interface-2, respectively; and f) Surf1 and Surf2, the receptor surface areas at the interface-1 and the interface-2 buried by βarr1. While Twist is a product of the intrinsic flexibility of βarr1, Rot, and Tilt describe the
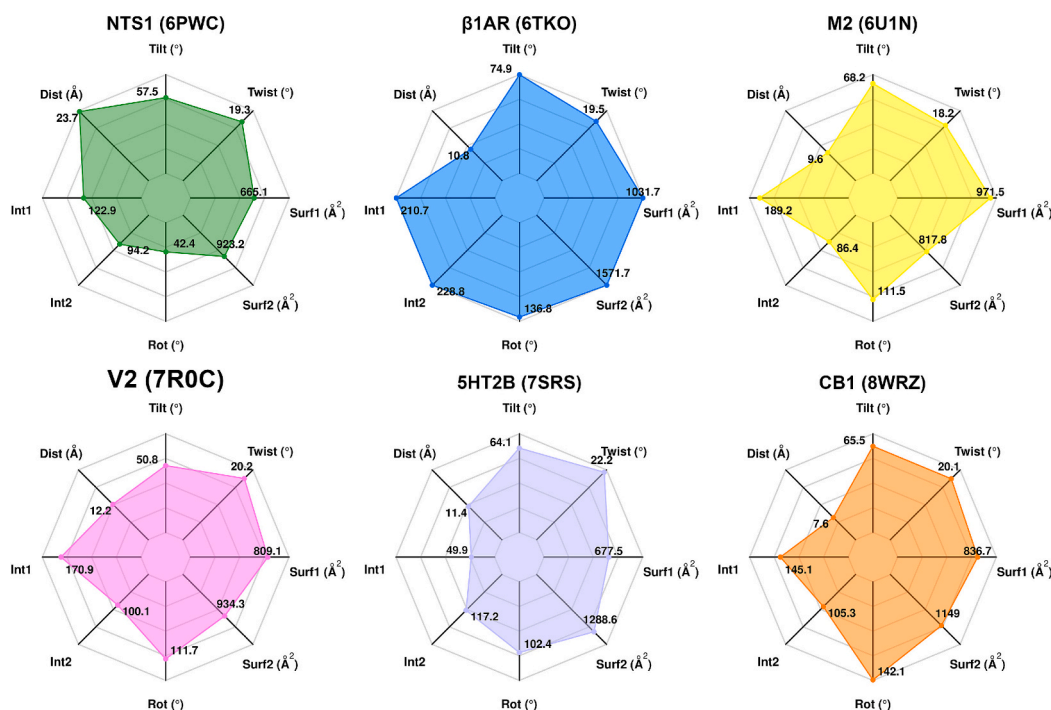
Fig. 3. Structural descriptors of six cryoEM βarr1-receptor complexes. Eight structural descriptors of six cryoEM complexes (NTSR1_6PWC, β1AR_6TKO, M2R_6U1N, V2R_7R0C, 5HT2BR_7SRS, CB1R_8WRZ) are shown in octagonal radar charts, in which each axis is a descriptor. The ranges of values over all systems are: Dist (7.6 Å–23.7 Å), Tilt (50.8°–74.9°), Twist (18.2°–22.2°), Rot (42.4°–142.1°), Int1 (49.9 %–210.7 %), Int2 (86.4 %–228.8 %), Surf1 (665.1Å²–1031.7Å²), and Surf2 (817.8Å²–1571.7Å²).

orientation of βarr1 with respect to the receptor (Fig. 3), Int1 and Surf1 describe, respectively, strength and shape/extension of the interface-1, Int2 and Surf2 describe strength and shape/extension of the interface-2, and Dist is inversely related to the tightness of the interface 2.

The combination of the eight descriptors in octagonal radar charts properly grasps structural similarities and differences in the cryoEM complexes between βarr1 and the six different GPCRs (Figs. 3 and 4, Table S2). Collectively, the shapes of the radar charts are quite divergent in the six systems (Fig. 3). Consistently with the Cα-RMSD data, the radar plot of NTSR1_6PWC displays the most divergent shape, characterized by singularly low and high values of Rot and Dist, respectively (Fig. 3). The complex β1AR_6TKO is the most divergent one from NTSR1_6PWC, holding all indices but Dist and Twist significantly higher compared to NTSR1_6PWC (Figs. 3 and 4, Table S2). The radar plots also highlight the rather small values of the Int2 and Surf2 indices for M2R_6U1R, Surf2 being singularly smaller than Surf1 (Fig. 3 and Table S2).

As for the Tilt angle, which is the inverse of the inclination of the βarr1 main-axis with respect to the receptor main axis, it is dictated by the interaction of βarr1 with the membrane and by the curvature of the latter. Indeed, for βarr1-GPCR complexes embedded in micelles of small size and high curvature (i.e. NTSR1_6PWC, V2R_7R0C, 5HT2BR_7SRS, and CB1R_8WRZ), βarr1 inclination is higher (low Tilt) compared to those complexes embedded in lipid nanodiscs (β1AR_6TKO and M2R_6U1N) or planar membranes (the forms simulated herein, Fig. 5). Incidentally, although embedded in detergent micelles, in 5HT2BR_7SRS and CB1R_8WRZ βarr1 is less tilted than in NTSR1_6PWC and V2R_7R0C (Figs. 3 and 4, Table S2 [37,40,41]).

In contrast to the high variability of all other indices, the inter-domain twist angle (Twist), which is an index of the intrinsic flexibility of βarr1, is almost invariant in the cryoEM complexes (on average 19.9 ± 1.33°, Fig. 3 and Table S2), being slightly lower than the twist angle in the βarr1-V2RCt complexes holding only the interface-1 (on average 22.7 ± 1.28°, Fig. 3 and Tables S1 and S2).

The structural plasticity of βarr1-GPCR complexes emerges also from

the analysis of the MD trajectories of WT and mutated V2R, which expand the possible shapes of the octagonal radar charts that, in this case, plot the average values of the eight descriptors computed over the MD trajectories (Fig. 5, S7, and S8). The radar chart of the V2R WT resembles that of β1AR_6TKO for the Tilt, Rot, and Int2 descriptors. V2R WT has a larger interface-2 (Surf2) compared to β1AR_6TKO, which, in turn, has the highest Surf2 among the cryoEM complexes (Figs. 3 and 5). Furthermore, in the simulated V2R WT, all indices but Twist and Dist are higher than those of the cryoEM complex V2R_7R0C, which, however, exhibits a singular inclination also among the cryoEM complexes (Figs. 3–5, S7, and S8). One of the possible causes of these divergences is the membrane shape, which is planar in MD simulations whereas it is markedly convex in V2R_7R0C. The high inclination of βarr1 interacting with micelles likely influences also the rotation of arrestin parallel to the membrane plane and weakens/reduces the interface-2. The inclination of βarr1 in all simulated complexes, especially those involving the V2R mutants, tends to be low (high Tilt value), whereas the indices accounting for tightness and shape/extension of the interface-2 (Int2 and Surf2, respectively) tend to be high. In the simulated complexes also the twist angle tends to be lower than those of the cryoEM complexes (the maximal median value, 16.67°, belongs to the WT, Fig. S8). In each of the five conformational ensembles βarr1 explores a wide variety of Twist values, which go from sporadic inactive-like values (i.e. around 0°) to various active-like values reaching 28.61° at maximum. Collectively, the establishment of core interactions (interface-2) in addition to tail interactions (interface-1) tends to lower the twist angle compared to the tail-only interactions.

All descriptors explore wide ranges of values in the conformational ensembles, the complexes involving the F229V mutant being more divergent from the other forms (Fig. 5, S7, and S8).

A singular behavior of the F229V forms, in particular the AVP-bound one, is the relatively high value of Dist, indicating detachment of the C-loop from H5 and changes in the interactions between β15/β16 hairpin and the small helix in IL2 (Fig. 5, S7, and S8). Moreover, F229V tends to frequently lose contact between the edge loops and the membrane, by
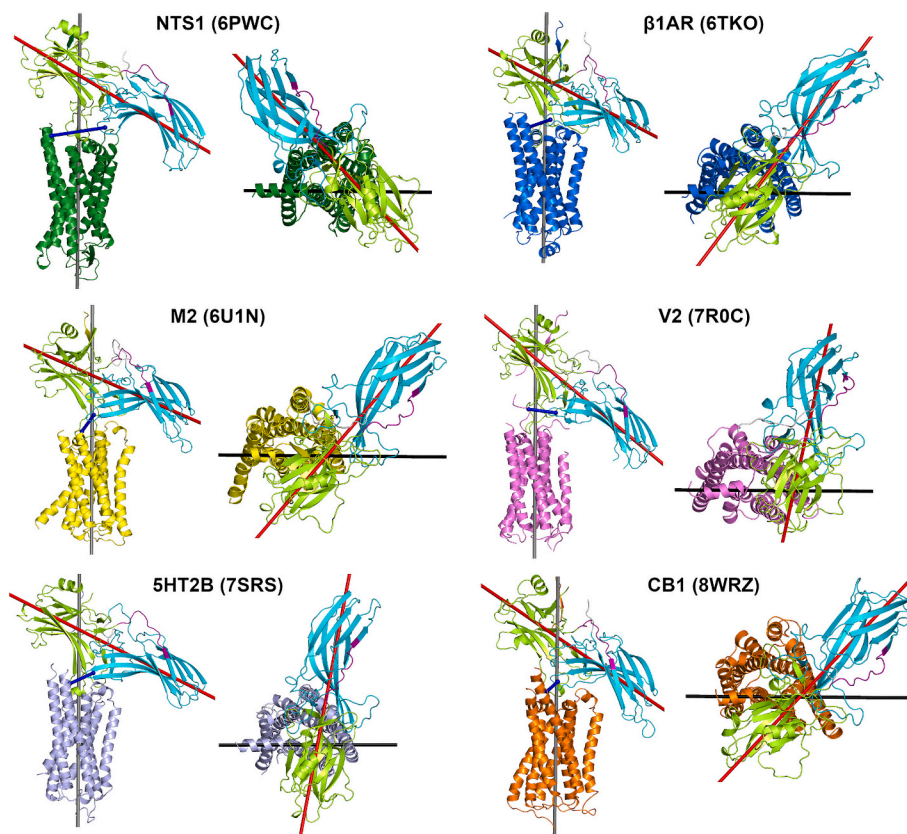
Fig. 4. Graphical representation of the Dist, Rot, and Tilt descriptors. The cartoon representations of six cryoEM complexes are shown, colored according to the different portions for βarr1 (see the legend to Fig. 1) and by receptor subtype, i.e. NTSR1: forest-green, β1AR: marine-blue, M2R: yellow, V2R: violet, 5HT2BR: light-blue, and CB1R: orange. Each complex is shown according to two views: perpendicular to the membrane plane with the cytosol on top, for the representation of the Dist and Tilt descriptors (left panel), and parallel to the membrane plane from the cytosol, for the representation of the Rot index. Dist is represented as a blue bar connecting two blue spheres centered on the centroid of the βarr1 C-loop and the closest receptor Cα-atom on H5. The main axes of the receptor (left panel) or H8 (right panel) are black, whereas the main axis of βarr1 is red. (For interpretation of the references to colour in this figure legend, the reader is referred to the web version of this article.)

exhibiting almost no inclination (Figs. 5, S1, S7-S9). Incidentally, while in the simulated WT and R137L mutant V2R, similarly to the majority of cryoEM complexes, the strength of the interface-1 (Int1) is higher than that of the interface-2 (Int2), the contrary happens for the two forms of the F229V mutant (Fig. 5 and Table S2).

The β18/β19 edge loop is highly mobile especially in the V2R mutants, as inferred by monitoring the distance between the Cα-atom centroid of the β14/β15 and β16/β17 loops and the centroid of the β18/β19 C-edge loop (Fig. S10).

Collectively, MD simulations of the five V2R forms show that changes in βarr1 inclination, interaction with the membrane, and conformational changes in the C-edge loops are all interconnected (Figs. 5, S7-S10).

Correlation analysis of the eight descriptors shows some linear trends in the merged pool of the six cryoEM βarr1-receptor complexes and the five Rframes concerning WT and mutated V2R (Fig. S11). Focusing on correlations with coefficients ≥0.70 in absolute values, the Twist index inversely correlates with the strength of both interfaces-1 and 2 (i.e. Int1 and Int2, respectively), indicating that higher values of the twist angle are favored by lower strength of the two interfaces. The index inversely correlates also with the Tilt index indicating that high values of twist angle correspond to high inclination of βarr1. The Tilt index of βarr1 is correlated to strength and shape/extension of the interface-2 (Int2 and Surf2, respectively), suggesting that high inclination of βarr1 weakens its interaction with the receptor core. In contrast, βarr1 rotation parallel to the membrane plane (Rot) is related to strength and shape/extension of the interface-1. For each of the two interfaces, strength and buried

receptor surface are correlated (Fig. S11). Some correlation also exists between the strength of the two interfaces, which may depend, in part, on the lariat loop that participates in both interfaces.

Collectively, the comparative analysis of high-resolution cryoEM structures highlights the extremely high variability in the ways the same arrestin, βarr1, recognizes different GPCRs or the same GPCR embedded in differently shaped membranes or hit by different functionally-active mutations, or found in different ligand-bound states. Tail and core interactions are likely independent from each other. Major divergences in the architectures of the complexes depend on βarr1 orientation, essentially caused by rotation parallel to the membrane plane and inclination with respect to the receptor main axis. While the strength/extension of tail interactions are linked to βarr1 rotation, strength/extension of core interactions are linked to βarr1 inclination.

3.1.4. Essential dynamics of βarr1 in complex with GPCRs

The central role of βarr1 rotation and tilting in determining the architecture of the complexes with GPCRs was corroborated by the analysis of collective motions. The pseudo-trajectories made of the cryoEM complexes were used as a reference framework for the analysis of the essential dynamics of the MD trajectories.

Remarkably, the first two collective motions inferred from the PCA on the trajectories of the five V2R forms indeed describe changes in either the Rot or the Tilt angles of βarr1 and overlap with the first two eigenvectors from the PCA on the pool of the cryoEM complexes, (Fig. 6). These results suggest that during MD simulations βarr1 experiences collective motions similar to the ones inferred from the divergent
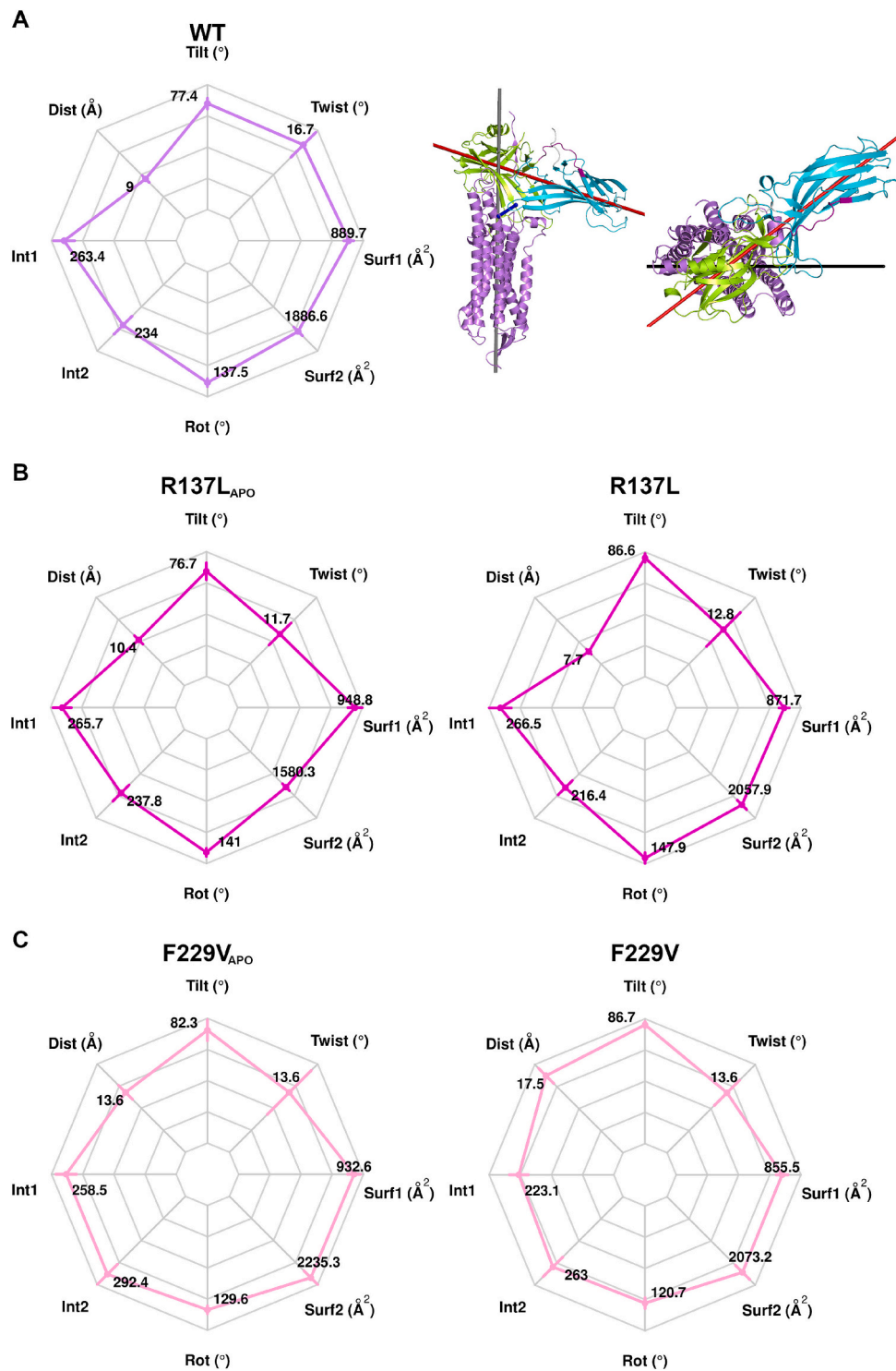
Fig. 5. Structural descriptors of the five simulated V2R forms. The radar charts plot the eight structural indices as averages over the trajectory frames of V2R WT, R137L, and F229V. The ranges of values overall systems are: Dist (7.7 ± 0.6 Å–17.5 ± 1.7 Å), Tilt (76.7 ± 6.2°–86.7 ± 2.3°), Twist (11.7 ± 2.5°–16.7 ± 2.8°), Rot (120.7 ± 6.8°–147.9 ± 6.7°), Int1 (223.1 ± 22.0 %–266.5 ± 26.0 %), Int2 (216.4 ± 27.0 %–292.4 ± 37.9 %), Surf1 (855.5 ± 47.4 Å²–948.8 ± 58.6 Å²), and Surf2 (1580.3 ± 96.6 Å²–2235.3 ± 188.0 Å²). In the top right panel 3D representations of the Dist, Rot, and Tilt indices are shown for the WT (see the legend to Fig. 4 for explanation). The same representations for the mutants are in Fig. S7.

βarr1 orientations in the six cryoEM complexes analyzed in this study. This is particularly true for F229V bound to AVP, for which PC1 and PC2 give high overlap, respectively, with PC1 and PC2 from the pool of the cryoEM structures, while for the other forms the overlap is reversed (Fig. 6). Both R137L forms give lower overlaps with the collective motions from the cryoEM pool compared to WT and both F229V forms,

suggesting rather singular dynamics triggered by mutation of the E/DRY arginine.

All together comparative PCA remarks the concept that the main collective motions of βarr1 as a whole include its rotation parallel to the membrane plane and its tilting with respect to the receptor main axis.
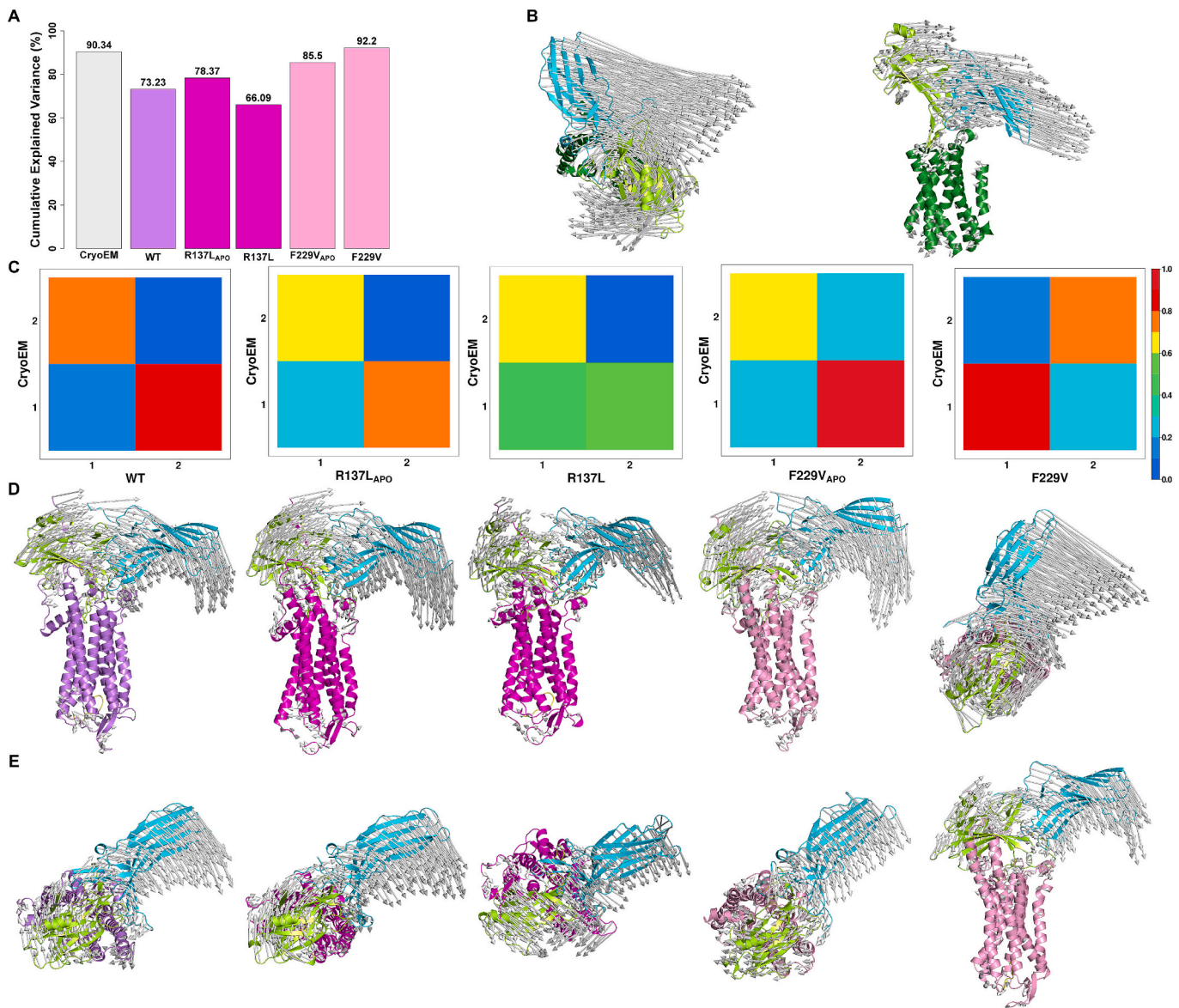
Fig. 6. Essential dynamics of βarr1-receptor complexes. Comparison between the essential motions computed on the ensemble of cryoEM complexes and those computed on the MD ensembles of five V2R forms. The covariance matrices were built on a pool of backbone atoms shared by the cryoEM and the MD complexes. The six cryoEM structures were first fitted on the receptor backbone atoms, and the frames of each trajectory were then fitted (at the level of receptors) on the average structure of the cryoEM ensemble. A. Bar plot of the cumulative variance explained by the first two eigenvectors of the cryoEM ensemble and the five MD trajectories is shown. B. The porcupine representations of PC1 (left) and PC2 (right) are shown on the cartoons of 6PWC (in forest-green colour). The extremities of the arrows correspond to the Cα-atoms of the structures 6PWC and 8WRZ for PC1 and 6PWC and 7R0C for PC2. C. The pairwise similarity (overlaps) between the first two eigenvectors of the cryoEM pool and each MD trajectory is shown. Porcupine representations of PC1 (D) and PC2 (E) concerning the five simulated βarr1-V2R complexes are shown. The extremities of the arrows in each system correspond to the trajectory frames with the largest displacement. As for the cartoon colors of the V2R forms, WT is lithium-violet, R137L is magenta, and F229V is pink. In all cartoon representations, the ND and CD of βarr1 are, respectively, lemon-green, and cyan. (For interpretation of the references to colour in this figure legend, the reader is referred to the web version of this article.)

3.2. Allosteric effects of AVP on βarr1 coupling to V2R WT and NSIAD mutants

The comparative structural/dynamics analysis shown in the previous sections highlighted divergences between AVP-bound forms of WT and NSIAD-linked mutants of V2R as well as between apo and AVP-bound forms of the same mutant (Figs. 5, S7-S10).

An important inference in this respect comes from the analysis of the geometrically stable substructures (GeoStaS), in other words, the dynamic protein domains that move as coherent units in a simulation [69], which highlighted the allosteric effect of AVP. Indeed, while in the two apo forms the intermolecular dynamic cluster of residues involves the C-

tail of the receptor (and also IL3 for F229V$_{APO}$) and the ND of βarr1, i.e. it essentially concerns the interface-1 (magenta cluster, Fig. 7), for the three AVP-bound states the intermolecular dynamic cluster involves the whole βarr1, the C-tail of the receptor participating in the interface-1, and a variable number of cytosolic receptor core regions participating in the interface-2 (red cluster, Fig. 7). The extension of such core regions is maximal in the F229V mutant, in which the whole cytosolic half of the receptor is involved (Fig. 7). The clear differences in βarr1-V2R dynamic coupling between apo and AVP-bound forms suggest the existence of an allosteric communication between the AVP docked in the extracellular end of the receptor and βarr1.

The analysis of the AVP-mediated structural sub-networks (i.e. AVP-
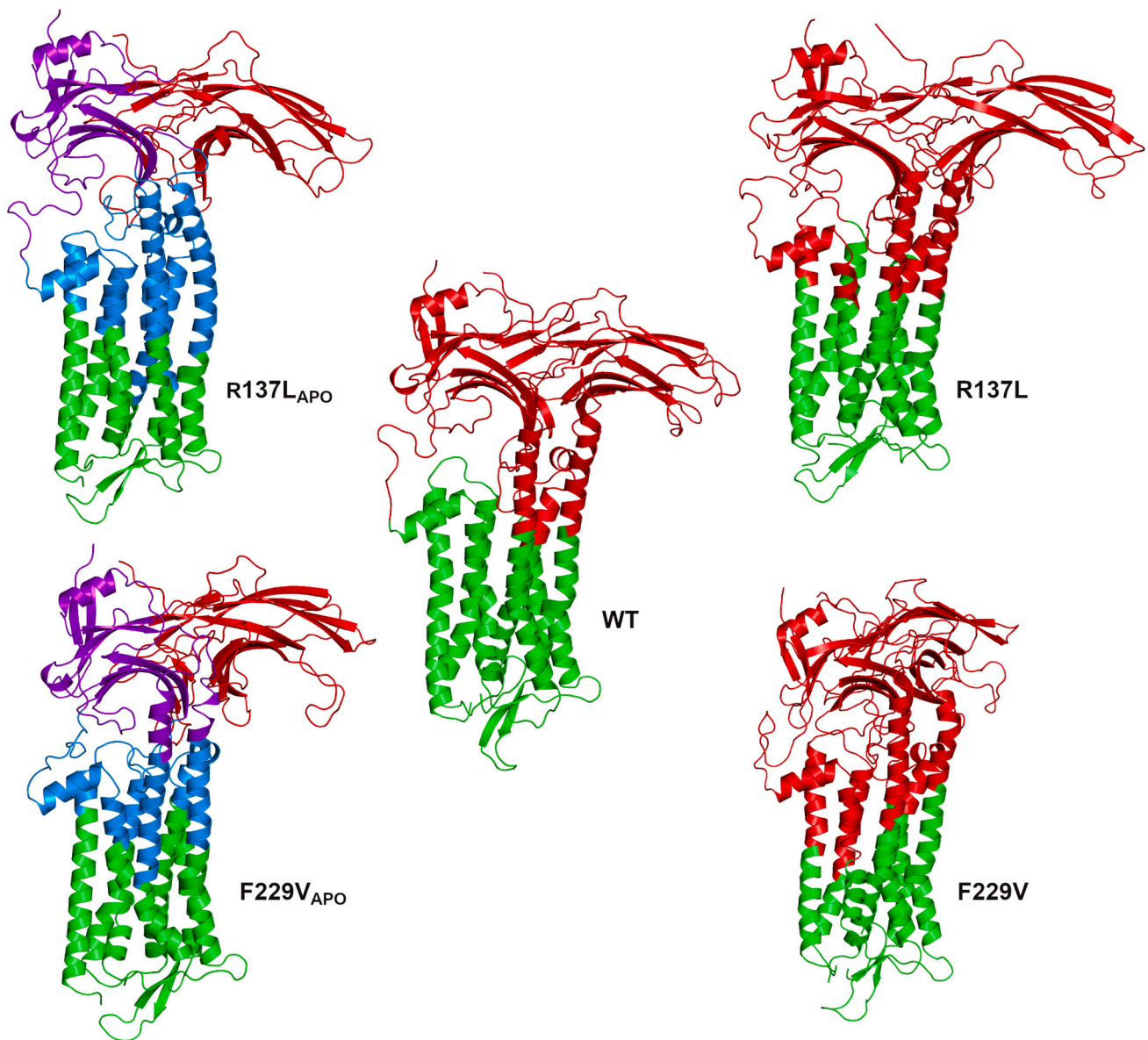
Fig. 7. Identification of dynamic sub-domains that move as coherent units in simulated V2R-βarr1 complexes. These sub-domains were identified using the geometrically stable substructures (GeoStaS) method, which groups atoms based on the similarity of their fluctuations using an agglomerative hierarchical clustering algorithm with a ward linkage criterion. For each trajectory, the number of sub-domains in which the atoms had to be partitioned was set according to the best Silhouette Width Index. The results of the GeoStaS analysis are visualized on the Rframe from each of the five conformational ensembles, with each sub-domain in a different colour. Inter-molecular subdomains are red (the most extended one) for WT, R137L, and F229V, whereas they are magenta for R137$_{APO}$ and F229V$_{APO}$. (For interpretation of the references to colour in this figure legend, the reader is referred to the web version of this article.)

V2R interaction shell) in WT, R137L, and F229V forms, highlights substantial similarities, especially in those nodes and links that involve the cyclic part of the peptide (Fig. S12A-C). In fact, Y2, F3, Q4, and N5 of AVP are connected with the same V2R nodes in all forms, Y2, F3, and Q4 being always hubs (i.e. nodes involved in at least four links) holding one or two links more in the WT compared to the two mutants. Major differences among the three forms concern the tail of AVP (i.e. P7, R8, and G9). In detail, a) P7 participates in the intermolecular interaction shell only in the two mutants and not the WT; b) R8 makes only one link common to the three forms (with D33 at position 1 × 28), and one link shared between WT and F229V (with E303 in E3) or between the two mutants (with R32 in the N-terminus); finally, c) G9 is a hub in WT and R137L but not in F229V, making two links common to WT and R137L but no link common to WT and F229V. While the cyclic part of AVP makes slightly stronger interactions (in terms of summation of link-strengths, which are expressed as percentages, see Eq. 1 in the Method

section) with WT V2R compared to the two mutants (127.61 %, 122.13 %, and 113.84 %, for WT, R137L, and F229V, respectively), the C-tail of AVP makes slightly stronger interactions with the two mutants compared to WT (32.07 %, 39.46 %, and 38.33 % for WT, R137L, and F229V, respectively). These effects remark the existence of a structural communication between the two mutation sites in the cytosolic half of the receptor and the AVP binding site in the extracellular half of the receptor. Collectively, while the cyclic part of AVP, in particular Y2, F3, and Q4, makes almost conserved links with the receptor, likely responsible for functional signal transfer to βarr1, the tail makes more variable links likely responsible for modulating signal transfer. This is consistent with evidence from *in vitro* experiments indicating that the main AVP pharmacophoric moiety for activating V2R is the Y2-F3 pair, while the rest of the peptide rather seems to be responsible for selectivity [47]. In line with that, the metapaths accounting for the most recurrent structural communication between the AVP binding site (including

AVP) and βarr1 highlight clear differences among the three AVP-bound forms (Fig. S12D). Common nodes in all metapaths are Y2-F3 on AVP and F288(6 × 51) and the highly conserved W284(6 × 48) on V2R, remarking their importance for the agonistic activity of AVP and the ability of GPCRs to transfer agonistic signals. In synthesis, in the WT, by involving the interface-2, the communication reaches $ND_{βarr1}$ via $CD_{βarr1}$, in R137L by involving the interface-2 the communication reaches interface-1, and, finally, in F229V by involving the interface-1 the communication reaches the $CD_{βarr1}$ via $ND_{βarr1}$. In this respect, by different pathways, agonist binding facilitates βarr1 trans-domain communication for WT and F229V but not for R137L (Fig. S12D). The allosteric communication between AVP and βarr1-coupling regions emerges also from the differences in buried surface area between the interfaces-1 and 2, which increases significantly (i.e. up to 1670 $Å^2$) in the AVP-bound states compared to the apo forms, reaching the maximal and minimal differences in F229V and $R137L_{APO}$, respectively (Fig. 5 and Table S2). Also, the extension of the buried interface-1 is higher in the apo forms compared to the AVP-bound ones, while on the contrary the extension of buried interface-2 is higher in the AVP bound forms compared to the apo ones (Fig. 5 and Table S2). $R137L_{APO}$ is singularly characterized by a significantly higher strength of the interface-1 compared to the interface-2 and by a minimal difference in the extension of the two interfaces (i.e. the difference between the Surf2 and Surf1 indices is 228.11 $Å^2$ and 1434.12 $Å^2$ in the apo and AVP-stimulated forms, respectively).

Determinations of BRET coupling of V2R WT, R137L, and F229V to βarr1 highlighted differences between the three forms. The coupling indices (Emax, for AVP-stimulated coupling, and Bmax for basal (AVP-independent) coupling) in BRET ratio units were computed from the concentration-response curves of AVP stimulation, which gave also the EC50 (or pEC50) values (Table S3) [18]. Surface expression (in the presence of βarr1) of the V2R forms, both in basal and AVP-stimulated conditions, was taken as a measure of receptor endocytosis (Table S3). For all WT and mutated V2R forms, the constitutive coupling to βarr1 was always significantly lower than the AVP-stimulated coupling (Table S3) [18]. The two NSIAD mutants were characterized by clearly different behaviors. While R137L showed slightly higher basal coupling but lower AVP-stimulated coupling to βarr1 than WT, F229V showed similar basal coupling but significantly higher AVP-stimulated coupling to βarr1 than WT (Table S3) [18]. In contrast, the R137L mutant showed basal and AVP-stimulated endocytosis higher than WT, whereas F229V showed constitutive and stimulated endocytosis similar to WT (Table S3). Notably, endocytosis may also hold an arrestin-independent component.

Interestingly, different combinations of the indices describing the structural complexes between βarr1 and the GPCRs (see Figs. 3 and 5) and of an index inferred from the GeoStatS method (GeoS, equal to the number of residues belonging to the intermolecular dynamic cluster) gave good linear correlations with the Bmax/Emax values concerning the simulated V2R forms. One of the best correlations with the lowest number of indices was obtained by the non-weighed summation of Dist and GeoS (R^2 = 0.96, Fig. S13), meaning that high βarr1-V2R coupling is linked to a combination of extension of the regions in intermolecular dynamic coupling and orientation of the β15/β16 βarr1 hairpin with respect to IL2 and H5 of the receptor. Remarkably, docking of the two-turn α-helix in IL2 onto the βarr1 cavity formed upon inter-domain twisting is one of the major contributors to the formation of βarr1-V2R core interactions.

Collectively, βarr1-V2R coupling relies on the interplay of internal degrees of freedom and orientation of βarr1 as well as the extent of the inter-molecular dynamically coupled regions. Signal transfer from the agonist-binding site to the cytosolic regions relies on specific amino acids, Y2 and F3, in the cyclic part of AVP. While in the absence of the agonist the intermolecular βarr1-V2R coupling concerns only the interface-1 that involves tail interactions, in the presence of the agonist the intermolecular coupling extends to the interface-2 that involves core

interactions. The extension of the latter (i.e. marked by Surf2) also increases under the allosteric effect of the agonist. Modulation of the shape/extension of the interface-2 primarily relies on βarr1 interaction with IL2 of the receptor.

4. Discussion

In this study, the dynamics of βarr1-V2R complexes was investigated by atomistic MD simulations. The V2R was used as a model system because the vast majority of structurally resolved complexes between βarr1 and GPCRs contain the V2RCt phosphopeptide, which provides GPCRs with high-affinity binding to βarrs [25,43]. Simulations of the R137L and F229V V2R CAMs were also aimed at inferring the determinants of their different coupling to βarr1, despite being both linked to NSIAD. Indeed, R137L showed slightly higher basal coupling but smaller AVP-stimulated coupling than WT, while F229V showed comparable basal coupling but significantly higher AVP-stimulated coupling than WT [18]. The increased basal coupling to βarr1 of R137L consistently resulted in increased βarr1-mediated endocytosis compared to the basal endocytosis of WT and F229V.

Simulations of the WT and functionally distinct mutants of the V2R in their apo and bound states contributed to expand the conformational ensembles of the βarr1-V2R system explored on the short time-scale (microsecond) of current simulations. The study did not intend to infer the process of βarr1-receptor recognition nor the steps of βarr1 activation by the receptor, which would require a special-purpose machine able to accelerate the execution of simulation and/or enhanced sampling methods [88,89]. The main goal was indeed to investigate the plasticity of the βarr1-V2R complexes and the allosteric communication inside those systems in the context of the existing high-resolution data. Cutting-edge structural analysis methods were employed on the purpose.

According to the current view, binding of βarr1 to those GPCRs that, like V2R, are phosphorylated in their C-tail would follow a sequential-step process, starting with recruitment of the receptor phosphorylated C-tail (i.e. formation of the interface-1, "hanging/tail conformation"), which induces the conformational changes necessary to form, in a second step, the secondary interface with the receptor core (i.e. formation of the interface-2, "core conformation") [3,26,27]. The interaction of βarr1 with the membrane via the C-edge loops would favor high-affinity core interactions [39]. Independently of the hypothetical sequential order of the events, engagement of both receptor tail and core is necessary for efficient arrestin activation [25]. The tail conformation is fully capable of promoting receptor internalization and receptor-mediated signaling, whereas desensitization of G protein activation is exclusively mediated by the receptor core-engaged βarr [29].

The V2RCt holds eight phosphorylation sites 346-RTPPSLGPQDE*S*CTTA*SS*LAKD-368 (i.e. typed in bold). Underlined-bold residues are those found phosphorylated in cryoEM determinations [38–40] and set phosphorylated in the present simulation study. Phosphoproteomics of purified V2R found high phosphorylation probability (>0.75) in the presence of AVP for almost all eight sites (T360 and S363 holding a probability slightly lower: 0.62 and 0.66, respectively) [38,40]. According to the barcode model, V2RCt holds the long *Px(x)PxxP* code with three phosphorylated residues, pS457, pT360, and pS363 (typed in bold-italic in the sequence above) likely required for high-affinity receptor-arrestin binding [20]. More recent alanine-scanning mutagenesis of individual or two/three phosphorylation sites in V2RCt showed the synergic relevance in βarr1 recruitment of the six sites found phosphorylated in the cryoEM density maps (underlined in the sequence above), while the two most N-terminal sites (T347 and S350) resulted irrelevant [90]. The role of phosphorylation patterns in βarr1 activation and receptor binding was investigated by atomic-level molecular simulations of the βarr1-V2RCt complex and site-directed spectroscopy [91]. Full phosphorylation (pp8), no phosphorylation, and 28 different patterns of mono, bi, and three-phosphorylations were

probed. It was inferred that patterns that favor binding differ from those that favor activation, selectively promoting a wide variety of βarr1 conformations and differently affecting arrestin sites implicated in scaffolding distinct signaling proteins [91]. The study also suggested that fully phosphorylated βarr1 exhibits maximal activation [91]. Yet, in that study, full phosphorylation was probed in the absence of the receptor core since control MD simulations on the βarr1-M2R/V2rCt complex holding the M2R core (M2R_6U1N) employed a penta-phosphorylated V2RCt (pp-1,2,8) [91]. Previous simulations of fully phosphorylated V2R-βarr1 complex showed that full phosphorylation of V2RCt with persistent interactions between pT347 and the singular cationic D site of βarr1 prevents the finger loop from interacting with the receptor H6 as in fully productive complexes [44]. Those results, together with the findings of the simulations on hexaphosphorylated V2R (i.e. with T347 and S350 non-phosphorylated, pp-1,2) reported in this study, suggest that the formation of a fully productive βarr1-V2R complex either occurs when T347 and S350 are not phosphorylated, or, in case of full phosphorylation, excludes the two N-terminal phosphorylated sites from interactions with the finger loop, letting it free to adopt different conformations/orientations and form high-affinity core interactions. These hypotheses are consistent with evidence that βarr1 binding to a fully phosphorylated receptor with a phosphorylation barcode identical to the isolated phosphopeptide is highly inefficient [25].

The analysis of the cryoEM complexes between βarr1 and several GPCRs highlighted the high dynamicity of βarr1, which undergoes conformational changes in its loops, rigid-body twisting of the two domains (Twist descriptor) as well as rigid-body rotation parallel to the membrane plane (Rot descriptor) and tilting with respect to the receptor main axis (Tilt descriptor) as a whole protein. As for the latter descriptor, the micelles in several cryoEM structure-determinations tend to exacerbate the inclination of arrestin (i.e. as seen for the NTSR1_6PWC and V2R_7R0C complexes). Independently of the amplitude of tilting, the important message from the structural analysis done in this study is that arrestin titling is a functionally relevant degree of freedom for arrestin to adapt to the different membrane curvatures encountered in its functional life when in complex with GPCRs, e.g. from almost planar plasma membranes to highly curved endocytic vesicles. The dynamism of βarr1-GPCR complexes was also inferred from a study on a Class-B receptor, based on the integration of the intermolecular Cβ-Cβ distances estimated by *in vivo* crosslinking with computational modeling [92].

Rotation and tilting of βarr1 appear to distinctly affect tail and core interactions: while rotation is linked to the structural features of the interface-1, inclination, which depends on membrane interaction, is linked to the structural features of the interface-2. Remarkably, rotation and tilting are the first two collective motions of βarr1 inferred from the pool of cryoEM complexes. Such collective motions overlap in the same or in an inverted order with the first two collective motions inferred from each of the five conformational ensembles of V2R simulated in this study. The relevant message is that the variegated orientations of βarr1 captured by cryoEM on different systems can be found in each of the simulated conformational ensembles of V2R. This is particularly remarkable and gives value to the study, considering also the relatively short simulation length and the indeterminations of integrative modeling. Singularly, F229V experiences higher-amplitude rotation than tilting, similar to the cryoEM pool but inversely to all other simulated V2R forms.

Motions and intrinsic flexibility of βarr1 depend on AVP-binding as a result of allosteric communications between agonist binding site and intracellular protein. Remarkably, the predicted structural communication between the agonist and βarr1 involves only two amino acids, Y2 and F3, out of 9 of the peptide, in perfect agreement with *in vitro* evidence that the agonist action of AVP depends essentially on that amino acid pair [47]. The long-range effects of AVP clearly emerge by comparing the AVP-bound and apo forms of R137L and F229V. In general, in the presence of AVP, the shape/extension of interface-2

increases, whereas that of the interface-1 diminishes compared to the apo forms. Moreover, the presence of AVP favors the extension of those βarr1 and V2R regions that move as coherent units, i.e. are dynamically coupled. Specifically, when AVP is bound to V2R, βarr1 as a whole becomes dynamically coupled to all receptor regions participating in both interfaces-1 and 2, whereas, when V2R is apo, the intermolecular dynamic coupling concerns only the interface-1. In other words, the intermolecular dynamic coupling of the receptor core regions requires the presence of the agonist. This is consistent with the evidence from single-molecule FRET that substantial βarr1 tail displacement by phosphorylated β2AR/V2RCt, a marker of activation, was only observed when the receptor was activated by the agonist [25]. The NSIAD mutant F229V exhibits the most extended AVP-induced dynamic coupling, compared to WT and R137L, which remarkably pairs with its highest BRET coupling. Thus, efficient AVP-stimulated coupling to βarr1 is linked to an interplay of interface-1 and interface-2, which makes βarr1 move as a whole, rather than as a bi-domain protein, coherently with the cytosolic half of the V2R involved in both tail and core interactions. Differently from the AVP-stimulated coupling, basal coupling to βarr1 aligns with an intermolecular-dynamic coupling limited to the interface-1. Moreover, while in all AVP-bound forms the extension of the two interfaces is unbalanced towards interface-2, in the apo forms, the difference in extension is reduced, becoming minimal in R137L_APO. This data suggests that the basal coupling to βarr1 and endocytosis of R137L would essentially depend on the formation of interface-1 (i.e. hanging/tail conformation). These results are consistent with previous findings that mutations of the E/DRY arginine in the α1b-AR increase the levels of receptor phosphorylation, thus remarking the communication between mutation site and receptor C-tail that participates in the interface-1 [93].

In conclusion, the present investigation provides significant insights into βarr1-receptor coupling. The combined information from cryoEM data and microsecond simulations highlighted the extremely high plasticity of βarr1-GPCR complexes, dependent on receptor type, state, and membrane environment. The multiple functions of βarr1 are likely determined by a complex interplay of βarr1 degrees of freedom, including intrinsic flexibility and collective motions both as a bi-domain protein and as a whole. The two major collective motions of the whole βarr1, consisting in rotation parallel to the membrane plane and inclination with respect to the receptor main axis, are distinctly linked to the two interfaces involved in tail and core interactions, which are independent from each other. Modulation of core interactions primarily relies on βarr1 interaction with the structurally conserved two-turn α-helix in IL2 of the receptor that docks into the βarr1 cavity formed upon interdomain twisting. Such cavity involves the central-crest loops and the C- and N-terms, respectively, of the β15 and β16 strands of βarr1. The primary role of the receptor IL2 in core interactions is consistent with evidence from structure determinations and molecular simulations [12,31,87].

The intermolecular dynamic coupling between βarr1 and V2R depends on the allosteric effect of AVP. While in the absence of AVP the dynamic coupling concerns only tail interactions, in the presence of AVP it involves both tail and core interactions. This suggests that while βarr1-receptor coupling at the interface-1 is a basal condition linked to both agonist-independent and agonist-dependent arrestin functions, coupling at the interface-2 depends on the agonist and is likely linked to desensitization of G protein signaling. The two spontaneous NSIAD-linked mutants R137L and F229V are exemplar in this respect. Indeed, while R137L, characterized by enhanced basal BRET coupling to βarr1 and endocytosis, in the absence of AVP is dynamically coupled to βarr1 exclusively at the interface-1, F229V, characterized by highly enhanced AVP-stimulated BRET coupling, in the presence of AVP shows both receptor tail and all core regions dynamically coupled to βarr1.

The huge lariat loop of βarr1, which participates both in the interface-1 and in the core interactions founding the interface-2, is likely to play a leading role in the modulation of the multiple βarr1 functions,

in line with ^{19}F NMR determinations highlighting the gate loop as central in the process of βarr1 activation [94].

The ability of the computational model to grasp the allosteric effects of an agonist on the dynamic coupling at the two interfaces can be exploited to infer the determinants of biased agonism towards βarr1-mediated signaling.

Funding

CRediT authorship contribution statement

Angelo Felline: Writing – review & editing, Visualization, Software, Methodology, Investigation, Formal analysis. **Luca Bellucci:** Writing – review & editing, Methodology, Investigation. **Vanessa Vezzi:** Writing – review & editing, Resources, Investigation. **Caterina Ambrosio:** Writing – review & editing, Resources, Investigation. **Susanna Cotecchia:** Writing – review & editing, Funding acquisition, Conceptualization. **Francesca Fanelli:** Writing – review & editing, Writing – original draft, Visualization, Resources, Methodology, Investigation, Funding acquisition, Formal analysis, Conceptualization.

Declaration of competing interest

The authors declare that they have no known competing financial interests or personal relationships that could have appeared to influence the work reported in this paper.

Appendix A. Supplementary data

Supplementary data to this article can be found online at https://doi.org/10.1016/j.ijbiomac.2024.137217.

References

[1] K.L. Pierce, R.T. Premont, R.J. Lefkowitz, Seven-transmembrane receptors, Nat. Rev. Mol. Cell Biol. 3 (9) (2002) 639–650.

[2] J.R. Hepler, A.G. Gilman, G-Proteins, Trends Biochem. Sci. 17 (10) (1992) 383–387.

[3] V.V. Gurevich, E.V. Gurevich, The molecular acrobatics of arrestin activation, Trends Pharmacol. Sci. 25 (2) (2004) 105–111.

[4] L.M. Luttrell, S.S. Ferguson, Y. Daaka, W.E. Miller, S. Maudsley, G.J. Della Rocca, F. Lin, H. Kawakatsu, K. Owada, D.K. Luttrell, M.G. Caron, R.J. Lefkowitz, Beta-arrestin-dependent formation of beta2 adrenergic receptor-Src protein kinase complexes, Science 283 (5402) (1999) 655–661.

[5] P.H. McDonald, C.W. Chow, W.E. Miller, S.A. Laporte, M.E. Field, F.T. Lin, R. J. Davis, R.J. Lefkowitz, Beta-arrestin 2: a receptor-regulated MAPK scaffold for the activation of JNK3, Science 290 (5496) (2000) 1574–1577.

[6] C.E. Alvarez, On the origins of arrestin and rhodopsin, BMC Evol. Biol. 8 (2008) 222.

[7] E. Alvarez-Curto, A. Inoue, L. Jenkins, S.Z. Raihan, R. Prihandoko, A.B. Tobin, G. Milligan, Targeted elimination of G proteins and Arrestins defines their specific contributions to both intensity and duration of G protein-coupled receptor signaling, J. Biol. Chem. 291 (53) (2016) 27147–27159.

[8] M. Grundmann, N. Merten, D. Malfacini, A. Inoue, P. Preis, K. Simon, N. Ruttiger, N. Ziegler, T. Benkel, N.K. Schmitt, S. Ishida, I. Muller, R. Reher, K. Kawakami, A. Inoue, U. Rick, T. Kuhl, D. Imhof, J. Aoki, G.M. Konig, C. Hoffmann, J. Gomeza, J. Wess, E. Kostenis, Lack of beta-arrestin signaling in the absence of active G proteins, Nat. Commun. 9 (1) (2018) 341.

[9] L.M. Luttrell, J. Wang, B. Plouffe, J.S. Smith, L. Yamani, S. Kaur, P.Y. Jean-Charles, C. Gauthier, M.H. Lee, B. Pani, J. Kim, S. Ahn, S. Rajagopal, E. Reiter, M. Bouvier, S.K. Shenoy, S.A. Laporte, H.A. Rockman, R.J. Lefkowitz, Manifold roles of beta-arrestins in GPCR signaling elucidated with siRNA and CRISPR/Cas9, Sci. Signal. 11 (549) (2018).

[10] M. O'Hayre, K. Eichel, S. Avino, X. Zhao, D.J. Steffen, X. Feng, K. Kawakami, J. Aoki, K. Messer, R. Sunahara, A. Inoue, M. von Zastrow, J.S. Gutkind, Genetic evidence that beta-arrestins are dispensable for the initiation of beta(2)-adrenergic receptor signaling to ERK, Sci. Signal. 10 (484) (2017).

[11] F. Fanelli, P.G. De Benedetti, Update 1 of: computational modeling approaches to structure-function analysis of G protein-coupled receptors, Chem. Rev. 111 (12) (2011) PR438–535.

[12] M. Seyedabadi, M. Gharghabi, E.V. Gurevich, V.V. Gurevich, Receptor-Arrestin interactions: the GPCR perspective, Biomolecules 11 (2) (2021).

[13] M. Birnbaumer, Vasopressin receptors, Trends Endocrinol. Metab. 11 (10) (2000) 406–410.

[14] G. Tamma, G. Procino, M. Svelto, G. Valenti, Cell culture models and animal models for studying the patho-physiological role of renal aquaporins, Cell. Mol. Life Sci. 69 (12) (2012) 1931–1946.

[15] P.G. Charest, G. Oligny-Longpre, H. Bonin, M. Azzi, M. Bouvier, The V2 vasopressin receptor stimulates ERK1/2 activity independently of heterotrimeric G protein signalling, Cell. Signal. 19 (1) (2007) 32–41.

[16] B.J. Feldman, S.M. Rosenthal, G.A. Vargas, R.G. Fenwick, E.A. Huang, M. Matsuda-Abedini, R.H. Lustig, R.S. Mathias, A.A. Portale, W.L. Miller, S.E. Gitelman, Nephrogenic syndrome of inappropriate antidiuresis, N. Engl. J. Med. 352 (18) (2005) 1884–1890.

[17] D. Bockenhauer, M.D. Penney, D. Hampton, W. van't Hoff, A. Gullett, S. Sailesh, D. G. Bichet, A family with hyponatremia and the nephrogenic syndrome of inappropriate antidiuresis, Am. J. Kidney Dis. 59 (4) (2012) 566–568.

[18] V. Vezzi, C. Ambrosio, M.C. Gro, P. Molinari, G. Sural, T. Costa, H.O. Onaran, S. Cotecchia, Vasopressin receptor 2 mutations in the nephrogenic syndrome of inappropriate antidiuresis show different mechanisms of constitutive activation for G protein coupled receptors, Sci. Rep. 10 (1) (2020) 9111.

[19] Q. Chen, J.J.G. Tesmer, G protein-coupled receptor interactions with arrestins and GPCR kinases: the unresolved issue of signal bias, J. Biol. Chem. 298 (9) (2022) 102279.

[20] X.E. Zhou, Y.Z. He, P.W. de Waal, X. Gao, Y.Y. Kang, N. Van Eps, Y.T. Yin, K. Pal, D. Goswami, T.A. White, A. Barty, N.R. Latorraca, H.N. Chapman, W.L. Hubbell, R. O. Dror, R.C. Stevens, V. Cherezov, V.V. Gurevich, P.R. Griffin, O.P. Ernst, K. Melcher, H.E. Xu, Identification of phosphorylation codes for Arrestin recruitment by G protein-coupled receptors, Cell 170 (3) (2017) 457–469.

[21] V.V. Gurevich, E.V. Gurevich, The structural basis of arrestin-mediated regulation of G-protein-coupled receptors, Pharmacol. Ther. 110 (3) (2006) 465–502.

[22] A. Mashukova, M. Spehr, H. Hatt, E.M. Neuhaus, Beta-arrestin2-mediated internalization of mammalian odorant receptors, J. Neurosci. 26 (39) (2006) 9902–9912.

[23] Z. Yang, F. Yang, D. Zhang, Z. Liu, A. Lin, C. Liu, P. Xiao, X. Yu, J.P. Sun, Phosphorylation of G protein-coupled receptors: from the barcode hypothesis to the flute model, Mol. Pharmacol. 92 (3) (2017) 201–210.

[24] S.R. Jung, C. Kushmerick, J.B. Seo, D.S. Koh, B. Hille, Muscarinic receptor regulates extracellular signal regulated kinase by two modes of arrestin binding, Proc. Natl. Acad. Sci. U. S. A. 114 (28) (2017) E5579–E5588.

[25] W.B. Asher, D.S. Terry, G.G.A. Gregorio, A.W. Kahsai, A. Borgia, B. Xie, A. Modak, Y. Zhu, W. Jang, A. Govindaraju, L.Y. Huang, A. Inoue, N.A. Lambert, V. V. Gurevich, L. Shi, R.J. Lefkowitz, S.C. Blanchard, J.A. Javitch, GPCR-mediated beta-arrestin activation deconvoluted with single-molecule precision, Cell 185 (10) (2022) 1661–1675 e16.

[26] A.H. Nguyen, A.R.B. Thomsen, T.J. Cahill 3rd, R. Huang, L.Y. Huang, T. Marcink, O.B. Clarke, S. Heissel, A. Masoudi, D. Ben-Hail, F. Samaan, V.P. Dandey, Y.Z. Tan, C. Hong, J.P. Mahoney, S. Triest, J.T. Little, X. Chen, R. Sunahara, J. Steyaert, H. Molina, Z. Yu, A. des Georges, R.J. Lefkowitz, Structure of an endosomal signaling GPCR-G protein-beta-arrestin megacomplex, Nat. Struct. Mol. Biol. 26 (12) (2019) 1123–1131.

[27] A.K. Shukla, G.H. Westfield, K. Xiao, R.I. Reis, L.Y. Huang, P. Tripathi-Shukla, J. Qian, S. Li, A. Blanc, A.N. Oleskie, A.M. Dosey, M. Su, C.R. Liang, L.L. Gu, J. M. Shan, X. Chen, R. Hanna, M. Choi, X.J. Yao, B.U. Klink, A.W. Kahsai, S.S. Sidhu, S. Koide, P.A. Penczek, A.A. Kossiakoff, V.L. Woods Jr., B.K. Kobilka, G. Skiniotis, R.J. Lefkowitz, Visualization of arrestin recruitment by a G-protein-coupled receptor, Nature 512 (7513) (2014) 218–222.

[28] A.R.B. Thomsen, B. Plouffe, T.J. Cahill 3rd, A.K. Shukla, J.T. Tarrasch, A.M. Dosey, A.W. Kahsai, R.T. Strachan, B. Pani, J.P. Mahoney, L. Huang, B. Breton, F. M. Heydenreich, R.K. Sunahara, G. Skiniotis, M. Bouvier, R.J. Lefkowitz, GPCR-G protein-beta-Arrestin super-complex mediates sustained G protein signaling, Cell 166 (4) (2016) 907–919.

[29] T.J. Cahill 3rd, A.R. Thomsen, J.T. Tarrasch, B. Plouffe, A.H. Nguyen, F. Yang, L. Y. Huang, A.W. Kahsai, D.L. Bassoni, B.J. Gavino, J.E. Lamerdin, S. Triest, A. K. Shukla, B. Berger, J.T. Little, A. Antar, A. Blanc, C.X. Qu, X. Chen, K. Kawakami, A. Inoue, J. Aoki, J. Steyaert, J.P. Sun, M. Bouvier, G. Skiniotis, R.J. Lefkowitz, Distinct conformations of GPCR-beta-arrestin complexes mediate desensitization, signaling, and endocytosis, Proc. Natl. Acad. Sci. U. S. A. 114 (10) (2017) 2562–2567.

[30] K. Chen, C. Zhang, S. Lin, X. Yan, H. Cai, C. Yi, L. Ma, X. Chu, Y. Liu, Y. Zhu, S. Han, Q. Zhao, B. Wu, Tail engagement of arrestin at the glucagon receptor, Nature 620 (7975) (2023) 904–910.

[31] N.R. Latorraca, J.K. Wang, B. Bauer, R.J.L. Townshend, S.A. Hollingsworth, J. E. Olivieri, H.E. Xu, M.E. Sommer, R.O. Dror, Molecular mechanism of GPCR-mediated arrestin activation, Nature 557 (7705) (2018) 452–456.

[32] K. Eichel, D. Jullie, B. Barsi-Rhyne, N.R. Latorraca, M. Masureel, J.B. Sibarita, R. O. Dror, M. von Zastrow, Catalytic activation of beta-arrestin by GPCRs, Nature 557 (7705) (2018) 381–386.

[33] J. Grimes, Z. Koszegi, Y. Lanoiselee, T. Miljus, S.L. O'Brien, T.M. Stepniewski, B. Medel-Lacruz, M. Baidya, M. Makarova, R. Mistry, J. Goulding, J. Drube, C. Hoffmann, D.M. Owen, A.K. Shukla, J. Selent, S.J. Hill, D. Calebiro, Plasma membrane preassociation drives beta-arrestin coupling to receptors and activation, Cell 186 (10) (2023) 2238–2255 e20.

[34] M. Han, V.V. Gurevich, S.A. Vishnivetskiy, P.B. Sigler, C. Schubert, Crystal structure of beta-arrestin at 1.9 angstrom: possible mechanism of receptor binding and membrane translocation, Structure 9 (9) (2001) 869–880.

[35] A.K. Shukla, A. Manglik, A.C. Kruse, K.H. Xiao, R.I. Reis, W.C. Tseng, D.P. Staus, D. Hilger, S. Uysal, L.Y. Huang, M. Paduch, P. Tripathi-Shukla, A. Koide, S. Koide,

W.I. Weis, A.A. Kossiakoff, B.K. Kobilka, R.J. Lefkowitz, Structure of active beta-arrestin-1 bound to a G-protein-coupled receptor phosphopeptide, Nature 497 (7447) (2013) 137–141.

[36] Q.T. He, P. Xiao, S.M. Huang, Y.L. Jia, Z.L. Zhu, J.Y. Lin, F. Yang, X.N. Tao, R. J. Zhao, F.Y. Gao, X.G. Niu, K.H. Xiao, J. Wang, C. Jin, J.P. Sun, X. Yu, Structural studies of phosphorylation-dependent interactions between the V2R receptor and arrestin-2, Nat. Commun. 12 (1) (2021) 2396.

[37] W. Yin, Z. Li, M. Jin, Y.L. Yin, P.W. de Waal, K. Pal, Y. Yin, X. Gao, Y. He, J. Gao, X. Wang, Y. Zhang, H. Zhou, K. Melcher, Y. Jiang, Y. Cong, X. Edward Zhou, X. Yu, H. Eric Xu, A complex structure of arrestin-2 bound to a G protein-coupled receptor, Cell Res. 29 (12) (2019) 971–983.

[38] Y. Lee, T. Warne, R. Nehme, S. Pandey, H. Dwivedi-Agnihotri, M. Chaturvedi, P. C. Edwards, J. Garcia-Nafria, A.G.W. Leslie, A.K. Shukla, C.G. Tate, Molecular basis of beta-arrestin coupling to formoterol-bound beta(1)-adrenoceptor, Nature 583 (7818) (2020) 862–866.

[39] D.P. Staus, H. Hu, M.J. Robertson, A.L.W. Kleinhenz, L.M. Wingler, W.D. Capel, N. R. Latorraca, R.J. Lefkowitz, G. Skiniotis, Structure of the M2 muscarinic receptor-beta-arrestin complex in a lipid nanodisc, Nature 579 (7798) (2020) 297–302.

[40] J. Bous, A. Fouillen, H. Orcel, S. Trapani, X. Cong, S. Fontanel, J. Saint-Paul, J. Lai-Kee-Him, S. Urbach, N. Sibille, R. Sounier, S. Granier, B. Mouillac, P. Bron, Structure of the vasopressin hormone-V2 receptor-beta-arrestin1 ternary complex, Sci. Adv. 8 (35) (2022) eabo7761.

[41] C. Cao, X. Barros-Alvarez, S. Zhang, K. Kim, M.A. Damgen, O. Panova, C. M. Suomivuori, J.F. Fay, X. Zhong, B.E. Krumm, R.H. Gumpper, A.B. Seven, M. J. Robertson, N.J. Krogan, R. Huttenhain, D.E. Nichols, R.O. Dror, G. Skiniotis, B. L. Roth, Signaling snapshots of a serotonin receptor activated by the prototypical psychedelic LSD, Neuron 110 (19) (2022) 3154–3167 e7.

[42] Y. Wang, L. Wu, T. Wang, J. Liu, F. Li, L. Jiang, Z. Fan, Y. Yu, N. Chen, Q. Sun, Q. Tan, T. Hua, Z.J. Liu, Cryo-EM structure of cannabinoid receptor CB1-beta-arrestin complex, Protein Cell 15 (3) (2024) 230–234.

[43] R.H. Oakley, S.A. Laporte, J.A. Holt, M.G. Caron, L.S. Barak, Differential affinities of visual arrestin, beta arrestin1, and beta arrestin2 for G protein-coupled receptors delineate two major classes of receptors, J. Biol. Chem. 275 (22) (2000) 17201–17210.

[44] L. Bellucci, A. Felline, F. Fanelli, Dynamics and structural communication in the ternary complex of fully phosphorylated V2 vasopressin receptor, vasopressin, and beta-arrestin 1, Biochim. Biophys. Acta Biomembr. 1862 (9) (2020) 183355.

[45] L. Wang, J. Xu, S. Cao, D. Sun, H. Liu, Q. Lu, Z. Liu, Y. Du, C. Zhang, Cryo-EM structure of the AVP-vasopressin receptor 2-G(s) signaling complex, Cell Res. 31 (8) (2021) 932–934.

[46] A. Sali, T.L. Blundell, Comparative protein modelling by satisfaction of spatial restraints, J. Mol. Biol. 234 (3) (1993) 779–815.

[47] J. Bous, H. Orcel, N. Floquet, C. Leyrat, J. Lai-Kee-Him, G. Gaibelet, A. Ancelin, J. Saint-Paul, S. Trapani, M. Louet, R. Sounier, H. Demene, S. Granier, P. Bron, B. Mouillac, Cryo-electron microscopy structure of the antidiuretic hormone arginine-vasopressin V2 receptor signaling complex, Sci. Adv. 7 (21) (2021).

[48] J.A. Ballesteros, H. Weinstein, Integrated methods for the construction of three-dimensional models and computational probing of structure-function relations in G protein-coupled receptors, Methods Neurosci. 25 (1995) 366–428.

[49] A.J. Kooistra, S. Mordalski, G. Pandy-Szekeres, M. Esguerra, A. Mamyrbekov, C. Munk, G.M. Keseru, D.E. Gloriam, GPCRdb in 2021: integrating GPCR sequence, structure and function, Nucleic Acids Res. 49 (D1) (2021) D335–D343.

[50] K. Fahmy, F. Jager, M. Beck, T.A. Zvyaga, T.P. Sakmar, F. Siebert, Protonation states of membrane-embedded carboxylic acid groups in rhodopsin and metarhodopsin II: a Fourier-transform infrared spectroscopy study of site-directed mutants, Proc. Natl. Acad. Sci. U. S. A. 90 (21) (1993) 10206–10210.

[51] K.P. Hofmann, P. Scheerer, P.W. Hildebrand, H.W. Choe, J.H. Park, M. Heck, O. P. Ernst, A G protein-coupled receptor at work: the rhodopsin model, Trends Biochem. Sci. 34 (11) (2009) 540–552.

[52] J.C. Phillips, R. Braun, W. Wang, J. Gumbart, E. Tajkhorshid, E. Villa, C. Chipot, R. D. Skeel, L. Kale, K. Schulten, Scalable molecular dynamics with NAMD, J. Comput. Chem. 26 (16) (2005) 1781–1802.

[53] U. Essmann, L. Perera, M.L. Berkowitz, T. Darden, H. Lee, L.G. Pedersen, A smooth particle mesh Ewald method, Journal of Chemical Physics 103 (19) (1995) 8577–8593.

[54] J.P. Ryckaert, G. Ciccotti, H.J.C. Berendsen, Numerical-integration of Cartesian equations of motion of a system with constraints - molecular-dynamics of N-alkanes, J. Comput. Phys. 23 (3) (1977) 327–341.

[55] M. Tuckerman, B.J. Berne, G.J. Martyna, Reversible Multiple Time Scale Molecular-Dynamics, J. Chem. Phys. 97 (3) (1992) 1990–2001.

[56] W.L. Jorgensen, J. Chandrasekhar, J.D. Madura, R.W. Impey, M.L. Klein, Comparison of simple potential functions for simulating liquid water, J. Chem. Phys. 79 (2) (1983) 926–935.

[57] W. Humphrey, A. Dalke, K. Schulten, VMD: Visual molecular dynamics, J. Mol. Graph. Model. 14 (1) (1996) 33–38.

[58] C. Barberis, B. Mouillac, T. Durroux, Structural bases of vasopressin/oxytocin receptor function, J. Endocrinol. 156 (2) (1998) 223–229.

[59] B. Mouillac, B. Chini, M.N. Balestre, J. Elands, S. Trumppkallmeyer, J. Hoflack, M. Hibert, S. Jard, C. Barberis, The binding-site of neuropeptide vasopressin V1a receptor - evidence for a major localization within transmembrane regions, J. Biol. Chem. 270 (43) (1995) 25771–25777.

[60] W. Huang, A. Manglik, A.J. Venkatakrishnan, T. Laeremans, E.N. Feinberg, A. L. Sanborn, H.E. Kato, K.E. Livingston, T.S. Thorsen, R.C. Kling, S. Granier, P. Gmeiner, S.M. Husbands, J.R. Traynor, W.I. Weis, J. Steyaert, R.O. Dror, B. K. Kobilka, Structural insights into micro-opioid receptor activation, Nature 524 (7565) (2015) 315–321.

[61] M. Seeber, A. Felline, F. Raimondi, S. Muff, R. Friedman, F. Rao, A. Caflisch, F. Fanelli, Wordom: a user-friendly program for the analysis of molecular structures, trajectories, and free energy surfaces, J. Comput. Chem. 32 (6) (2011) 1183–1194.

[62] A. Felline, S. Conti, M. Seeber, M. Cecchini, F. Fanelli, Wordom update 2: a user-friendly program for the analysis of molecular structures and conformational ensembles, Comput Struct, Biotechnol. J. 21 (2023) 1390–1402.

[63] A. Felline, M. Seeber, F. Fanelli, PSNtools for standalone and web-based structure network analyses of conformational ensembles, Comput Struct, Biotechnol. J. 20 (2022) 640–649.

[64] I. Navizet, F. Cailliez, R. Lavery, Probing protein mechanics: residue-level properties and their use in defining domains, Biophys. J. 87 (3) (2004) 1426–1435.

[65] R. Lavery, S. Sacquin-Mora, Protein mechanics: a route from structure to function, J. Biosci. 32 (5) (2007) 891–898.

[66] S. Sacquin-Mora, E. Laforet, R. Lavery, Locating the active sites of enzymes using mechanical properties, Proteins-Structure Function and Bioinformatics 67 (2) (2007) 350–359.

[67] M. Munz, J. Hein, P.C. Biggin, The role of flexibility and conformational selection in the binding promiscuity of PDZ domains, PLoS Comput. Biol. 8 (11) (2012) e1002749.

[68] M. Gerstein, R.B. Altman, Average core structures and variability measures for protein families: application to the immunoglobulins, J. Mol. Biol. 251 (1) (1995) 161–175.

[69] J. Romanowska, K.S. Nowinski, J. Trylska, Determining geometrically stable domains in molecular conformation sets, J. Chem. Theory Comput. 8 (8) (2012) 2588–2599.

[70] A. Amadei, A.B. Linssen, H.J. Berendsen, Essential dynamics of proteins, Proteins 17 (4) (1993) 412–425.

[71] E.F. Pettersen, T.D. Goddard, C.C. Huang, G.S. Couch, D.M. Greenblatt, E.C. Meng, T.E. Ferrin, UCSF Chimera–a visualization system for exploratory research and analysis, J. Comput. Chem. 25(13) (2004) 1605–12.

[72] R.L. Dunbrack Jr., M. Karplus, Backbone-dependent rotamer library for proteins. Application to side-chain prediction, J Mol Biol 230 (2) (1993) 543–574.

[73] J.W. Ponder, F.M. Richards, Tertiary templates for proteins. Use of packing criteria in the enumeration of allowed sequences for different structural classes, J Mol Biol 193 (4) (1987) 775–791.

[74] S. Vishveshwara, K.V. Brinda, N. Kannan, Protein structure: insights from graph theory, J. Theor. Comput. Chem. 1 (2002) 187–211.

[75] A. Felline, M. Seeber, F., Fanelli, webPSN v2.0: a webserver to infer fingerprints of structural communication in biomacromolecules, Nucleic Acids Res. 48 (W1) (2020) W94–W103.

[76] F. Raimondi, A. Felline, M. Seeber, S. Mariani, F. Fanelli, A mixed protein structure network and elastic network model approach to predict the structural communication in biomolecular systems: the PDZ2 domain from tyrosine phosphatase 1E as a case study, J. Chem. Theory Comput. 9 (2013) 2504–2518.

[77] S. Vishveshwara, A. Ghosh, P. Hansia, Intra and inter-molecular communications through protein structure network, Curr. Protein Pept. Sci. 10 (2) (2009) 146–160.

[78] K.V. Brinda, S. Vishveshwara, A network representation of protein structures: implications for protein stability, Biophys. J. 89 (6) (2005) 4159–4170.

[79] A. del Sol, H. Fujihashi, D. Amoros, R. Nussinov, Residues crucial for maintaining short paths in network communication mediate signaling in proteins, Mol. Syst. Biol. 2 (2006) 0019.

[80] A. del Sol, H. Fujihashi, D. Amoros, R. Nussinov, Residue centrality, functionally important residues, and active site shape: analysis of enzyme and non-enzyme families, Protein Sci. 15 (9) (2006) 2120–2128.

[81] E.W. Dijkstra, A note on two problems in Connexion with graphs, Numer. Math. 1 (1959) 269–271.

[82] S.A. Vishnivetskiy, J.A. Hirsch, M.G. Velez, Y.V. Gurevich, V.V. Gurevich, Transition of arrestin into the active receptor-binding state requires an extended interdomain hinge, J. Biol. Chem. 277 (46) (2002) 43961–43967.

[83] S.A. Vishnivetskiy, C. Schubert, G.C. Climaco, Y.V. Gurevich, M.G. Velez, V. V. Gurevich, An additional phosphate-binding element in arrestin molecule - implications for the mechanism of arrestin activation, J. Biol. Chem. 275 (52) (2000) 41049–41057.

[84] S.K. Vishnivetskiy, C.L. Paz, C. Schubert, J.A. Hirsch, P.B. Sigler, V.V. Gurevich, How does arrestin respond to the phosphorylated state of rhodopsin? J. Biol. Chem. 274 (17) (1999) 11451–11454.

[85] O.B. Goodman, J.G. Krupnick, F. Santini, V.V. Gurevich, R.B. Penn, A.W. Gagnon, J.H. Keen, J.L. Benovic, beta-arrestin acts as a clathrin adaptor in endocytosis of the beta(2)-adrenergic receptor, Nature 383 (6599) (1996) 447–450.

[86] S.A. Vishnivetskiy, C. Zheng, M.B. May, P.C. Karnam, E.V. Gurevich, V. V. Gurevich, Lysine in the lariat loop of arrestins does not serve as phosphate sensor, J. Neurochem. 156 (2020) 435–444.

[87] Y. Kang, X.E. Zhou, X. Gao, Y. He, W. Liu, A. Ishchenko, A. Barty, T.A. White, O. Yefanov, G.W. Han, Q. Xu, P.W. de Waal, J Ke, M.H. Tan, C. Zhang, A. Moeller, G.M. West, B.D. Pascal, N. Van Eps, L.N. Caro, S.A. Vishnivetskiy, R.J. Lee, K. M. Suino-Powell, X. Gu, K. Pal, J. Ma, X. Zhi, S. Boutet, G.J. Williams, M. Messerschmidt, G. Gati, N.A. Zatsepin, D. Wang, D. James, S. Basu, S. Roy-Chowdhury, C.E. Conrad, J. Coe, H. Liu, S. Lisova, C. Kupitz, I. Grotjohann, R. Fromme, Y. Jiang, M. Tan, H. Yang, J. Li, M. Wang, Z. Zheng, D. Li, N. Howe, Y. Zhao, J. Standfuss, K. Diederichs, Y. Dong, C.S. Potter, B. Carragher, M. Caffrey, H. Jiang, H.N. Chapman, J.C. Spence, P. Fromme, U. Weierstall, O.P. Ernst, V. Katritch, V.V. Gurevich, P.R. Griffin, W.L. Hubbell, R.C. Stevens, V. Cherezov, K. Melcher, H.E. Xu, Crystal structure of rhodopsin bound to arrestin by femtosecond X-ray laser, Nature 523 (7562) (2015) 561–567.

[88] D.E. Shaw, P. Maragakis, K. Lindorff-Larsen, S. Piana, R.O. Dror, M.P. Eastwood, J. A. Bank, J.M. Jumper, J.K. Salmon, Y. Shan, W. Wriggers, Atomic-level characterization of the structural dynamics of proteins, Science 330 (6002) (2010) 341–346.

[89] R.O. Dror, T.J. Mildorf, D. Hilger, A. Manglik, D.W. Borhani, D.H. Arlow, A. Philippsen, N. Villanueva, Z. Yang, M.T. Lerch, W.L. Hubbell, B.K. Kobilka, R. K. Sunahara, D.E. Shaw, Signal transduction. Structural basis for nucleotide exchange in heterotrimeric G proteins, Science 348 (6241) (2015) 1361–1365.

[90] H. Dwivedi-Agnihotri, M. Chaturvedi, M. Baidya, T.M. Stepniewski, S. Pandey, J. Maharana, A. Srivastava, N. Caengprasath, A.C. Hanyaloglu, J. Selent, A. K. Shukla, Distinct phosphorylation sites in a prototypical GPCR differently orchestrate beta-arrestin interaction, trafficking, and signaling, Sci. Adv. 6 (37) (2020) eabb8368.

[91] N.R. Latorraca, M. Masureel, S.A. Hollingsworth, F.M. Heydenreich, C. M. Suomivuori, C. Brinton, R.J.L. Townshend, M. Bouvier, B.K. Kobilka, R.O. Dror, How GPCR phosphorylation patterns orchestrate Arrestin-mediated signaling, Cell 183 (7) (2020) 1813–1825 e18.

[92] Y. Aydin, T. Bottke, J.H. Lam, S. Ernicke, A. Fortmann, M. Tretbar, B. Zarzycka, V. V. Gurevich, V. Katritch, I. Coin, Structural details of a class B GPCR-arrestin complex revealed by genetically encoded crosslinkers in living cells, Nat. Commun. 14 (1) (2023) 1151.

[93] A. Scheer, T. Costa, F. Fanelli, P.G. De Benedetti, S. Mhaouty-Kodja, L. Abuin, M. Nenniger-Tosato, S. Cotecchia, Mutational analysis of the highly conserved arginine within the Glu/asp-Arg-Tyr motif of the alpha(1b)-adrenergic receptor: effects on receptor isomerization and activation, Mol. Pharmacol. 57 (2) (2000) 219–231.

[94] R. Zhai, Z. Wang, Z. Chai, X. Niu, C. Li, C. Jin, Y. Hu, Distinct activation mechanisms of beta-arrestin-1 revealed by (19)F NMR spectroscopy, Nat. Commun. 14 (1) (2023) 7865.